

Geochemistry and petrogenesis of Soltan Maidan basalts (E Alborz, Iran): Implications for asthenosphere-lithosphere interaction and rifting along the N margin of Gondwana

Morteza Derakhshi ^{a,*} Habibollah Ghasemi ^b Laicheng Miao ^c

^a Department of Geology, Urmia Branch, Islamic Azad University, Urmia, Iran

^b Faculty of Earth Science, Shahrood University of Technology, Shahrood, Iran

^c Institute of Geology and Geophysics, Chinese Academy of Sciences, Beijing, China

* Corresponding author.

Tel.: +984432719900; fax: +984432622738; P.O. Box 969

E-mail address: mortezaderakhshi78@yahoo.com (M. Derakhshi)

Abstract

Soltan Maidan Basaltic Complex with thickness up to about 1300 m is located in the eastern Alborz zone, north of Iran. This complex is dominantly composed of transitional to mildly alkaline basaltic lava flows, agglomerates and tuffs, together with a few thin sedimentary interlayers. Field geological evidence and study of palynomorph assemblages in the shale interlayer show Late Ordovician to Early Late Silurian ages. Chondrite- and primitive-mantle normalized multi-element patterns of Soltan Maidan basalts demonstrate enrichment in highly incompatible elements relative to less incompatible ones and their patterns are most similar to

OIB. Trace elemental and Sr-Nd isotopic compositions indicate interaction and mixing of asthenospheric mantle source (OIB-type) with enriched subcontinental lithospheric mantle components (EM1-type). This asthenosphere-lithosphere interaction occurred in an extensional continental setting, which resulted in opening of the Paleotethys Ocean in the north of Gondwana during the Late Silurian to Middle Devonian.

Keywords: Soltan Maidan basalts, geochemistry, asthenosphere-lithosphere interaction, Paleotethys, Alborz

1. Introduction

The Iran plate refers to a collection of smaller blocks, of probable Gondwanan or peri-Gondwanan affinity, which made up part of the larger Cimmerian continent during evolution of the Paleotethys and Neotethys oceans (Sengör, 1987). Phases of plate separation and collision along the northern and southern margins of Iran are defined by potential passive-margin sequences, obducted ophiolites, and unconformable detrital formations (Horton et al., 2008). Although the existence and precise locations of Paleotethys (north Iranian) and Neotethys (south Iranian) suture zones are debated, most reconstructions indicate that closure of Paleotethys and collision along the northern margin occurred in Triassic or Jurassic times, whereas Neotethys was consumed between Arabia and Iran during the Late Cretaceous or Cenozoic (e.g., Horton et al., 2008; Rolland et al., 2009; Zanchi et al., 2009; Muttoni et al., 2009; Shafaii Moghadam and Stern, 2014; Saccani et al., 2015).

Generally, Ordovician to Early-Middle Devonian magmatic activities in different parts of Iran are interpreted as rift-related magmatic events that led to the

formation of the Paleotethys Ocean (e.g., Jenny, 1977; Stampfli, 1978; Berberian and King, 1981; Boulin, 1991; Stampfli et al., 1991; Alavi, 1996; Lasemi, 2001; Ghasemi and Derakhshi, 2008; Bagheri and Stampfli, 2008; Derakhshi and Ghasemi, 2014, 2015; Ayati, 2015; Hosseini et al., 2015). Also, study of Paleozoic ophiolites of Iran by Shafaii Moghadam and Stern (2014) indicates that all of them are remnants of Paleotethys Ocean and have a range of ages from Devonian to Permian.

Soltan Maidan Basaltic Complex (SMBC) with Late Ordovician-Early Late Silurian age is located in the eastern Alborz zone (Fig. 1). It represents the most important, thick and voluminous Lower Paleozoic volcanic activity in Iran. The thickness of this complex varies from 436 to 1286 m and is dominantly comprised of basaltic to basaltic-andesite rocks which are associated with a few sedimentary interlayers. The SMBC overlies the Upper Ordovician Ghelli Formation that consists mainly of olive-gray, silty shale and gray shale (Fig. 2). Study of Ghelli Formation by Ghavidel-Syooki et al. (2011) and Ghavidel-Syooki (2016) showed a relatively shallow marine, platformal depositional environment and a 'North Gondwana Domain' affinity for this formation.

Most information about the evolution stages of the Paleotethys have been obtained based on stratigraphy, paleontology and tectonic studies. However, igneous activities related to the formation of the Paleotethys have not yet been studied in detail. In this study, we present a set of whole-rock geochemical and isotopic data for Soltan Maidan basalts and biostratigraphic (palynological) age of the sedimentary interlayers in the SMBC. Using these data, we evaluate the nature of the mantle source, the role of asthenosphere-lithosphere interaction in the origin of the Soltan Maidan volcanic rocks, and also age of the complex and its relationship with the Paleotethys evolution.

2. Field geology

The Alborz mountain system, which is characterized by having a Precambrian basement, extends from the Lesser Caucasus of Armenia and Azerbaijan Republics in the northwest to the Paropamisus Mountains of northern Afghanistan to the east, and forms a composite polyorogenic belt (Alavi, 1996). The Alborz mountain system in northern Iran, with a generally E-W trend, divided into western, central, and eastern parts. The SMBC crops out in the eastern part of Alborz and northwest to northeast of Shahrud city (Fig. 1).

We studied three main outcrops of the SMBC, including (a) Kaludar Valley (b) Cheshmeh-Seyed Valley and (c) around the village of Khoshyeilaq, which are located in the northwest, north and northeast of Shahrud, respectively (Fig. 1). The SMBC comprises basaltic lava flows, agglomerates and tuffs, which is accompanied with a few thin sedimentary interlayers of shale, siltstone, sandstone and conglomerate (Fig. 2). Field geological evidence indicated that this complex was accumulated in both subaerial and submarine environments (Derakhshi and Ghasemi, 2015).

The best and most complete outcrop of the SMBC in the study area with thickness up to about 1300 m and includes at least 50 basaltic lava flows has been identified in the Cheshmeh-Seyed Valley (Fig. 2). The SMBC overlies the Upper Ordovician Ghelli Formation and is disconformably overlain by the Padeha Formation belong to the Early-Middle Devonian.

3. Analytical methods

Thirty samples were analyzed for whole-rock major and trace elements after fusion of 0.2 g of rock powder with 1.5 g LiBO₂ and dissolved in 100 ml 5% HNO₃ by inductively coupled plasma spectroscopy (ICP) at SGS Analytical

Laboratories, Toronto, Canada. Major elements and some trace elements including Ba, Sr, Y, Zn, and Zr were analyzed via Inductively Coupled Plasma-Atomic Emission Spectrometry (ICP-AES). A further suite of trace elements include Co, Cs, Cu, Ga, Hf, Nb, Ni, Rb, Ta, Th, U, V, and rare earth elements (REEs) were analyzed by Coupled Plasma-Mass Spectrometry (ICP-MS). Major elements analyzed with detection limit of 0.01 % and trace elements analyzed with detection limits between 0.05 to 10 ppm (U, Pr, Eu, Gd, Tb, Dy, Ho, Er, Tm, Lu 0.05 ppm, Cs, Th, Y, La, Ce, Nd, Sm, Yb 0.1 ppm, Rb 0.2 ppm, Ta, Co 0.5 ppm, Hf, Nb, Ga 1 ppm, Ni, V, Zn, Cu 5 ppm, Ba, Sr 10 ppm). Major and trace element compositions are listed in Table 1.

Whole rock powders for Sr and Nd isotopic analyses were dissolved in Savillex Teflon screw-top capsule after being spiked with the mixed ^{87}Rb - ^{84}Sr and ^{149}Sm - ^{150}Nd tracers prior to $\text{HF} + \text{HNO}_3 + \text{HClO}_4$ dissolution. Rb, Sr, Sm and Nd were separated using the classical two-step ion exchange chromatographic method and measured using a Triton Plus multi-collector thermal ionization mass spectrometer at Institute of Geology and Geophysics, Chinese Academy of Science (IGG, CAS). The total procedural blank was less than 300 pg for Rb-Sr and 100 pg for Sm-Nd. The $^{87}\text{Sr}/^{86}\text{Sr}$ and $^{143}\text{Nd}/^{144}\text{Nd}$ ratios were corrected for instrumental mass fractionation by normalizing to $^{86}\text{Sr}/^{88}\text{Sr} = 0.1194$ and $^{146}\text{Nd}/^{144}\text{Nd} = 0.7219$, respectively. The international standard samples (NBS987 and JNdi-1) were used to evaluate instrument stability during the period of data collection. Replicate analyses of the NBS987 and JNdi-1 standards gave $^{87}\text{Sr}/^{86}\text{Sr} = 0.710243 \pm 0.000011$ and $^{143}\text{Nd}/^{144}\text{Nd} = 0.512115 \pm 0.000012$, respectively. Detailed procedures for the Sr-Nd isotopic measurements are given in Yang et al. (2010).

Palynological study was carried out on 6 surface samples from the shale units of the C1 and C2 (Fig. 2) and slides pertaining to this study prepared in the palynology laboratory of the Geological Survey of Iran, and the National Iranian

Oil Company, Tehran. Palynomorphs were extracted from the sedimentary samples by using the standard palynological technique of treatment in HCl and HF to remove carbonates and silicates, respectively, and density separation of the organic residues in 30 ml of saturated zinc bromide solution. Organic residues were then sieved through 20 μ m nylon mesh sieves. In general, most samples contain well-preserved and abundant palynomorph taxa, including acritarchs, miospores, scolecodonts, and chitinozoans.

4. Biostratigraphy

Since the SMBC is stratigraphically located between the two formations of Ghelli (Late Ordovician) and Padeha (Early to Middle Devonian), this complex is generally considered Silurian in age and the precise age of the complex is not known. Here we should mention that K-Ar dating by Jenny (1977) and also our attempt for dating (in the present study) have yielded a wide range of isotopic ages from Precambrian to Mesozoic, which is not compatible with the clear stratigraphic position of the SMBC.

Ghavidel-Syooki et al. (2011) on the basis of palynomorph assemblages and stratigraphic relationships in the Khoshyeilaq area has indicated that SMBC is not younger than Gorstian (Early Late Silurian) in age. In our study, due to the existence of a complete exposure of the SMBC in the Cheshmeh-Seyed Valley section (Fig. 2), we have examined the palynomorph assemblages in the sedimentary interlayers to determine the age of the complex. As a result, based on the palynomorph assemblages (Fig. 3a-l) in the shale units of the C1 and C2 (Fig. 2), a Late Ordovician (Hirnantian) age is assigned to these two interlayers. We have also used some data from Ghavidel-Syooki et al. (2011) for correlation and to determine the age of palynomorph assemblages in the shale units of the C3 and C4

(Fig. 2). Their results (on the equivalent shale units with C3 and C4 in the present study) in the Khoshyeilaq area has been indicated typical middle Silurian forms of acritarch assemblages, and they pointed out that SMBC is not younger than Gorstian (early Ludlow, early late Silurian). Hence, the combination of our results with those described by Ghavidel-Syooki et al. (2011) indicates Late Ordovician to Early Late Silurian ages for SMBC.

5. Petrography

Soltan Maidan basalts are generally dark gray to greenish dark grey in color and display moderate to high degrees of alteration. These lavas that are uniform in composition include subaphyric to porphyritic basalt and basaltic andesite (Fig. 4a-d). Ophitic, subophitic, poikilitic, seriate, glomeroporphyritic (Fig. 4a) and amygdaloidal (Fig. 4d) textures are also present, but are less abundant. Amygdales are well developed at the upper and lower parts of the lava flows.

Labradorite plagioclase (up to 25 %) and augite (up to 10 %) are present as phenocrysts, and the groundmass is composed of plagioclase, augite, glass, and Fe-Ti oxides (Fig. 4a-b and d). Also olivine that completely replaced by secondary minerals is present in a few samples (Fig. 4c). The Fe-Ti oxides in the investigated rocks include magnetite, ilmenite and titanomagnetite in decreasing order of abundance.

Secondary alteration is a widespread phenomenon in the studied rocks, so that minerals such as chlorite (Fig. 4d), calcite (Fig. 4c and d), epidote, quartz, albite, sphene, and clay minerals are common. It was also found that all glasses have been converted to chlorite as a stable crystalline phase. Also, electron microprobe analyses (EMPA) of plagioclases by Derakhshi et al. (2015) indicated extensive albitization and replacement of labradorite by albite.

6. Results

6.1. Geochemistry

Whole-rock major and trace element concentrations of 30 samples are presented in Table 1. Soltan Maidan volcanic rocks have a relatively wide compositional range in major oxides: SiO_2 =46.7-55.2 wt% (average=50.1 wt%), $\text{Fe}_2\text{O}_{3(\text{t})}$ =8.38-14.9 wt%, MgO =2.8-10.1 wt% (average=5.4 wt%), CaO =4.01-9.43 wt%, Al_2O_3 =12.4-16.3 wt%, TiO_2 =1.61-3.34 wt%, P_2O_5 =0.16-0.48 wt% and $\text{K}_2\text{O}+\text{Na}_2\text{O}$ from 2.43 to 6.54 wt%.

All of the incompatible trace elements (such as REEs, Nb, Ta, and Hf) correlate positively with SiO_2 and Zr contents, whereas compatibles (such as Cr and Ni) correlate positively with MgO (not shown). These trends are accompanied by low MgO, Ni (6-218 ppm) and Co (28.8-68 ppm) contents and show the role of the fractional crystallization and also suggest that the volcanic rocks are not primary in origin. Also, the La/Ce (between 0.39 and 0.49, with an average of 0.45) and Ce/Sm (between 5.65 and 9.43, with an average of 7.42) ratios of these samples appear to be higher than those of primitive mantle (0.39 and 4.0, respectively, Sun and McDonough, 1989), reflecting their derivation from a fertile mantle source.

Because of the mobility of K_2O and Na_2O in the altered rocks, we prefer not use the TAS diagram and instead the Zr/ TiO_2 versus Nb/Y (Winchester and Floyd, 1977) diagram was chosen for rock classification. As shown in Fig. 5, studied volcanic samples are plotted in subalkaline-alkaline basaltic fields and mostly near the boundary line between them. Also, variations of La/Lu ratios versus La (Fig. 6) indicate variations in degrees of partial melting in the source. Indeed, variations in degrees of partial melting and subsequent fractional crystallization of melt have led to the transitional to mildly alkaline nature of the magma.

6.2. Sr-Nd isotopic results

Sr and Nd isotopic abundances and ratios are given in Table 2. All initial isotopic ratios, on the basis of the ages of the palynomorph assemblages in the shale interlayers of the SMBC (see section 4), are corrected to 430 Ma. The rocks of the SMBC show isotope compositions: $^{87}\text{Sr}/^{86}\text{Sr} = 0.704138\text{--}0.706733$, $^{143}\text{Nd}/^{144}\text{Nd} = 0.512440\text{--}0.512746$, $^{87}\text{Sr}/^{86}\text{Sr}_{\text{initial}} = 0.704062\text{--}0.705697$, $^{143}\text{Nd}/^{144}\text{Nd}_{\text{initial}} = 0.512064\text{--}0.512315$, $\epsilon_{\text{Nd}} = -3.86$ to $+2.10$, and $\epsilon_{\text{Sr}} = -5.14$ to $+31.69$. Relatively low $^{143}\text{Nd}/^{144}\text{Nd}$ values of these samples indicating they were probably derived from an enriched mantle source, similar to an EM1 or EM2 component (discussed later).

7. Discussion

7.1. Fractional crystallization and crustal contamination

Before using isotopic and geochemical data of these basaltic magmas to constrain their potential mantle sources, it is necessary to evaluate the role of both fractional crystallization and crustal contamination in modifying the chemical compositions of the magmas. Continental basalts often have more complex geochemical signatures than oceanic basalts, that reflect the additional involvement of the continental lithosphere in the magma generation process (e.g., Hawkesworth et al., 1988; Carlson, 1991; Saunders et al., 1992). As the input of crustal materials will increase the content of most lithophile elements, such as Rb, Ba and Sr, decrease high field strength elements, such as Nb, Ta and Zr, and decrease La/Nb, Ti/Y, Ba/Rb and Sr/Rb ratios as well (Brewer et al., 1992; Turner et al., 1996). It must be pointed out, however, that incompatible trace element ratios (Such as

Zr/Nb and Nb/La) are not strongly fractionated from each other either during partial melting or fractional crystallization (Jung and Hoernes, 2000).

Fig. 7 provides commonly used parameters for identifying fractional crystallization (FC) and assimilation and fractional crystallization (AFC) processes. As Nb versus Zr plot (Fig. 7a) shows slight AFC and remarkable FC processes. But, samples in Y versus Zr (Fig. 7b) and Nb/La versus SiO₂ (Fig. 7c) plots display consistent FC process. These diagrams suggest that FC would dominate the evolutionary trends. Also, clinopyroxene-melt thermobarometry by Derakhshi et al. (2015) indicated that magmatic fractionation took place in the shallow magma chamber(s).

Significant differences in trace element ratios between Soltan Maidan basalts and the continental crust show that these basalts have not been significantly affected by crustal contamination. For example, the average Zr/Nb, Ba/Nb, Th/Nb, Ba/La and Rb/Nb ratios of Soltan Maidan basaltic rocks are significantly lower than the values for the average continental crust (Table 3). In addition, average La/Nb, Ba/Th and Th/La ratios of these rocks are lower than those of the continental crust (Table 3). Also, if the magmas were significantly contaminated by the crustal materials, a negative Nb anomaly should be observed in the primitive mantle-normalized pattern (Fig. 9, discussed later), because the negative Nb anomaly is a diagnostic parameter for the AFC process.

Fractional crystallization and crustal contamination may also be assessed using Nd-Sr isotopic ratios plotted against 1/Sr and 1/Nd (Fig. 8a-b) and SiO₂ contents (Fig. 8c-d). Fig. 8 suggests that the Soltan Maidan basalts are genetically related by low-pressure fractional crystallization and do not support crustal assimilation or AFC processes.

As a result, there is no obvious isotopic and geochemical evidence for significant crustal contamination, and therefore the chemical compositions of these basaltic rocks reflect those of the mantle source regions.

7.2. Magma source

Chondrite- and primitive-mantle normalized multi-element patterns for the Soltan Maidan basaltic samples are shown in Fig. 9. In these spider diagrams, the average normalized composition of Soltan Maidan basalts display general enrichments in highly incompatible elements relative to less incompatible ones and they are plotted between OIB and E-MORB patterns. However, our samples are relatively depleted in some incompatible elements compared with typical OIB patterns. The normalized trace-element abundance patterns also show an affinity with OIB compositions. OIB is generally considered to be plume-related and thought to be the product of partial melting of several components within the mantle (Zindler and Hart, 1986). As shown in Fig. 9, there are no depletions in the high field strength elements, such as Nb and Ta, and samples patterns are more similar to the patterns of OIB and are more enriched than the E-MORB. Also, there is no significant negative Eu anomaly when normalized with primitive mantle (Fig. 9b), and the negative Sr anomaly in these diagrams is related to the intense alteration of the plagioclases in the post-eruption stage.

Discrimination diagrams of Zr/Y versus Zr (Pearce and Norry, 1979) and Ti/100-Zr-Y*3 (Pearce and Cann, 1973) for Soltan Maidan volcanic rocks show that all of the samples plot in the within-plate (continental rift) setting (Fig. 10a and b). Likewise, Nb/La versus Ti/Y diagram indicates an ocean-island basalt (OIB) affinity for samples (Fig. 10c), and it is compatible with chondrite- and primitive-mantle normalized multi-element patterns that are more similar to OIB. These

results suggest that lower contents of REE and other incompatible elements in the normalized multi-element patterns (relative to OIB, in Fig. 9a and 9b) is probably related to higher degrees of partial melting at shallower depths.

On the $^{143}\text{Nd}/^{144}\text{Nd}$ (and ϵ_{Nd}) versus $^{87}\text{Sr}/^{86}\text{Sr}$ diagram (Fig. 11), the fields for the mantle end-member components of DM, MORB, HIMU, EM1 and EM2 (Zindler and Hart, 1986) and our samples together with OIB are shown for comparison. As shown in Fig. 11, samples are located near the present day GHUR value and show a trend to EM1 (enriched mantle) end-member component. The EM1 end-member component has been considered to be related to an ancient subcontinental lithospheric mantle (SCLM) (Song et al., 1990; Basu et al., 1991) or to the metasomatized lower portion of an old SCLM (Tatsumoto and Nakamura, 1991). Furthermore, bulk silicate earth-like Nd and Sr isotopic compositions are also observed in xenoliths derived from SCLM (Menzies et al., 1987).

Our samples have $^{87}\text{Sr}/^{86}\text{Sr}$ values varying from 0.704138 to 0.706733 (Table 2 and Fig. 11), remarkably lower than those characteristics of EM2 compositions. The EM2 end-member component is usually considered to be indicative of an enriched mantle source metasomatized by subduction-related melt/fluids (e.g., Weaver, 1991). Hence, on the basis of the $^{143}\text{Nd}/^{144}\text{Nd}$ versus $^{87}\text{Sr}/^{86}\text{Sr}$ diagram (Fig. 11), SCLM may be contributed as a source for basaltic rocks in study area, but, as discussed earlier, this is in contrast to the OIB signatures of magma source.

In Table 3, incompatible trace element ratios of Soltan Maidan basalts and different mantle and crustal sources, including primitive mantle, N-MORB, E-MORB, continental crust, HIMU-, EM1-, EM2- and -OIB are given for comparison. The results of this comparison show remarkable similarities between trace element ratios of Soltan Maidan basalts and EM1-OIB source. As their Zr/Nb, La/Nb, Ba/Nb, Ba/Th, Th/La and Ba/La ratios, with averages of 9.46, 1.06, 14.6, 122, 0.12 and 13.4 respectively, are in the range of values for EM1-OIB

source (Table 3). Also their Th/Nb and Rb/Nb ratios are near the EM1-OIB values, and are distinct from other major chemical reservoirs. In fact, the chemical signatures of the SCLM are imparted into the plume-derived melts through the plume-lithosphere interaction (Song et al., 2008; He et al., 2010). Therefore, Soltan Maidan basalts have been generated by mixing of a subcontinental lithospheric mantle (EM1 end-member component) and a melt that originated from an asthenospheric mantle source. Indeed, the petrogenesis of these basalts is most consistent with melting of asthenospheric mantle source with some contributions from SCLM.

7.3. Tectono-magmatic model

Iranian and Arabian plates formed a coherent unit during the Paleozoic and were separated from the Turan plate in the north by Paleotethys Ocean (Karimpour et al., 2010). During this time period, Alborz was located in the northern Gondwana Domain (Ghavidel-Syooki and Winchester-Seeto, 2002; Stampfli et al., 2002; Ghavidel-Syooki, 2008; Horton et al., 2008; Ghavidel-Syooki, 2016).

Evidence show that Soltan Maidan volcanism leading to >1000 m lava flows may have been resulted from a continental rift setting near the Paleotethys suture zone. This is the most important and voluminous magmatic event in the Alborz zone corresponding to the initiation of extension of Paleotethys. As discussed in section 4, the SMBC is generally considered Silurian in age, however, palynomorph assemblages in the sedimentary interlayers indicate that the onset of the volcanic activity occurred in the Late Ordovician time and lasted to the Early Late Silurian. During this period of time, studied area and other parts of Alborz zone were dominated by an extensional tectonic regime. The transitional to mildly alkaline nature of samples may also show intense crustal thinning in the area,

where decompression can take place and explain the Lower Paleozoic volcanic activity in the SMBC as well as the geochemical characteristics. The alkaline magma can be generated in an extensional continental setting, however, in regions with large amounts of crustal extension, transitional and tholeiitic types may be common (Wilson, 1989). Also, the Soltan Maidan lavas have moderate TiO_2 contents (between 1.61 and 3.34 wt%, with an average of 2.35 wt%) and represent magmas generated from a slightly shallower mantle source than high-Ti magmas. In general, basalts with high-Ti content have commonly been interpreted as evidence for the involvement of asthenospheric mantle source components in the petrogenesis of the basaltic magmas (Barry et al., 2003; He et al., 2010). Therefore, it seems probable that these basalts were generated by shallow melting of asthenospheric mantle source mixed with different amounts of melts from SCLM, and the TiO_2 would decrease with increasing amounts of SCLM addition.

In Fig. 12, we present a tectono-magmatic model for the Late Ordovician to Middle Devonian time in the study area. In this model, volcanic eruption in the study area started in the Late Ordovician. The presence of columnar joints formed in the first lava flow in the westernmost outcrop (i.e., Kaludar Valley) show that the beginning of volcanic eruption in this part occurred in a subaerial environment. In addition, presence of some pillow lavas and columnar joints accompanied with subaerial and shallow marine sediment interlayers in the different parts of the SMBC (As shown in Fig. 2) indicate both subaerial and submarine environments during the formation of the complex. Volcanic activity in the study area has continued at least until the Early Late Silurian (see section 4). According to Alavi (1996), Ordovician was the time of initiation of continental extension in the Alborz, and rifting event that led to the formation of the Paleotethys Ocean lasted up to Early-Middle Devonian times. Also, Stampfli et al. (2002) pointed out that seafloor spreading took place in the Late Silurian or Early Devonian. The presence

of an erosional surface at the top of the SMBC overlaid by sandstones and conglomerates of Padeha Formation (belonging to Early-Middle Devonian) as disconformity (As shown in Fig. 2) show that volcanic activity probably continued after the Early Late Silurian. It seems that the continental breakup and opening of Paleotethys should have taken place after the end of Soltan Maidan volcanism and synchronous or after the erosional event at the top of the SMBC.

Soltan Maidan basalts have transitional to mildly alkaline nature, LREE-enriched patterns, EM1 and OIB-like geochemical signatures and generated in a continental rift setting. Also, the magmatism represented by these basalts is coeval and genetically associated with the lithosphere thinning beneath the area (Fig. 12). We suggest that contamination of asthenospheric magmas by lithosphere-derived melts probably has played an important role at the asthenosphere-lithosphere boundary. As the upwelling of the asthenospheric mantle plume or asthenospheric melts generated by lithospheric thinning in an extensional regime has provided enough heat energy for thermal erosion of the subcontinental lithospheric mantle at this boundary. In this case, interaction and mixing of asthenospheric mantle source (OIB-type) with enriched subcontinental lithospheric mantle components (EM1-type) has likely generated the Soltan Maidan basalts.

8. Conclusions

Field-relationships, palynological, geochemical and Sr-Nd isotopic studies of the Soltan Maidan Basaltic Complex led us to the following conclusions:

- 1) Based on the palynomorph assemblages in the sedimentary interlayers, the onset of the volcanic activity occurred in the Late Ordovician time and continued at least until the Early Late Silurian. The presence of an erosional surface at the top

of the SMBC indicates that volcanic activity may have been continued during the Late Silurian.

2) Soltan Maidan basalts are transitional to mildly alkaline in nature, and generated in a within-plate (continental rift) setting. Variations in degrees of partial melting and also fractional crystallization in the magma chamber(s) at shallower depths have played significant role in the magma genesis and subsequent magmatic evolution. Furthermore, these basalts have not been significantly affected by crustal contamination.

3) The observed trace element and Sr-Nd isotopic characteristics show similarities between Soltan Maidan basalts and EM1-component-bearing, OIB-like compositions. Therefore, we suggest that interaction and mixing of asthenospheric mantle materials (OIB-type) with enriched subcontinental lithospheric mantle components (EM1-type) has played a significant role at the asthenosphere-lithosphere boundary.

4) It appears that Soltan Maidan volcanism was synchronous with continental extension event, prior to oceanic crust inception and continental drift, in the northern Gondwana domain. Also, the final continental breakup and opening of Paleotethys seems to have taken place synchronous with a broad erosional surface at the top of the SMBC and/or deposition of the Padeha Formation during the Late Silurian to Middle Devonian.

Acknowledgements

This research is part of the PhD thesis by M.D. at Shahrood University of Technology. This study was jointly supported by the Shahrood University of Technology and the Iran National Science Foundation, Presidential Office, Deputy of Science and Technology (Grant No. 90004893). We would like to thank Prof.

Mohammad Ghavidel-Syooki for preparation and study of the palynological samples. We thank authorities at the Institute of Geology and Geophysics, Chinese Academy of Sciences (IGG, CAS), Beijing, China for assistance with Sr-Nd isotope analyses. Finally, we are grateful to the Department of Geology, Urmia Branch, Islamic Azad University, Urmia, Iran for allowing us the use of their facilities.

References

- Alavi, M., 1996. Tectonostratigraphic synthesis and structural style of the Alborz mountain system in Northern Iran. *J. Geodyn.* 21, 1-33.
- Ayati, F., 2015. Geochemistry, petrogenesis and tectono-magmatic setting of the basic magmatism in Ardekan and Isfahan, Central Iran. *J. Afr. Earth. Sci.* 108, 64-73.
- Bagheri, S., Stampfli, G.M., 2008. The Anarak, Jandaq and Posht-e-Badam metamorphic complexes in central Iran: New geological data, relationships and tectonic implications. *Tectonophysics* 451, 123-155.
- Barry, T.L., Saunders, A.D., Kempton, P.D., Windley, B.F., Pringle, M.S., Dorjnamjaa, D., Saandar, S., 2003. Petrogenesis of Cenozoic basalts from Mongolia: evidence for the role of asthenospheric versus metasomatised lithospheric mantle sources. *J. Petrol.* 44, 55-91.
- Basu, A.R., Wang, J.W., Huang, W.K., Xie, G.H., Tatsumoto, M., 1991. Major element, REE and Pb, Nd and Sr isotopic geochemistry of Cenozoic volcanic rocks of eastern China: implication for their origin from suboceanic type mantle reservoirs. *Earth Planet. Sci. Lett.* 105, 149-169.
- Berberian, F., King, G.C.P., 1981. Towards a paleogeography and tectonic evolution of Iran. *Can. J. Earth Sci.* 5, 101-117.
- Boulin, J., 1991. Structures in Southwest Asia and evolution of the eastern Tethys. *Tectonophysics* 196, 211-268.
- Brewer, T.S., Hergt, J.M., Hawkesworth, C.J., 1992. Coats land dolerites and the generation of Antarctic continental flood basalts. In: Story, B.C., Alabaster, T.R., Pankhurst, R.J. (Eds.), *Magmatism and the Causes of Continental Break-up*. *Geol Soc Spec Publ.* 68, 185-208.

- Carlson, R.W., 1991. Physical and chemical evidence on the cause and characteristics of flood basalt volcanism. *Aust. J. Earth Sci.* 38, 535-544.
- Derakhshi, M., Ghasemi, H., 2014. Ordovician-Devonian magmatism in the north of Shahrood: implication for long lived rifting of Paleotethys in Eastern Alborz. *Petrology* (quarterly research journal published by University of Isfahan, Isfahan, Iran). 5(18), 105-122 (in Persian).
- Derakhshi, M., Ghasemi, H., 2015. Soltan Maidan Complex (SMC) in the eastern Alborz structural zone, northern Iran: magmatic evidence for Paleotethys development. *Arabian J. Geosci.* 8, 849-866.
- Derakhshi, M., Ghasemi, H., Toksoy Koksall, F., 2015. Mineral chemistry and thermobarometry of Soltan Maidan basalts. *Iran J. Crystallogr. Mineral.* 23(2), 253-264 (in Persian).
- Dong, Y., Xiao, L., Zhou, H., Du, J., Zhang, N., Xiang, H., Wang, C., Zhao, Z., Huang, H., 2010. Volcanism of the Nanpu Sag in the Bohai Bay Basin, Eastern China: Geochemistry, petrogenesis, and implications for tectonic setting. *J. Asian Earth Sci.* 39, 173-191.
- Ghasemi, H., Derakhshi, M., 2008. Mineralogy, geochemistry and role of olivine mechanical separation in generation of Lower Paleozoic igneous rocks in Shirgesht area, NW of Tabas, Central Iran. *Iran J. Crystallogr. Mineral.* 16(2), 207-224 (in Persian).
- Ghavidel-Syooki, M., 2008. Palynostratigraphy and palaeogeography of the Upper Ordovician Gorgan Schists (Southeastern Caspian Sea), Eastern Alborz Mountain Ranges, Northern Iran. *Comunicações Geológicas*. 95, 123-155.
- Ghavidel-Syooki, M., 2016. Cryptospore and trilete spore assemblages from the Late Ordovician (Katian-Hirnantian) Ghelli Formation, Alborz Mountain Range, Northeastern Iran: Palaeophytogeographic and palaeoclimatic implications. *Rev. Palaeobot. Palynol.* doi: 10.1016/j.revpalbo.2016.04.006 (in press).
- Ghavidel-Syooki, M., Winchester-Seeto, T., 2002. Biostratigraphy and palaeogeography of Late Ordovician chitinozoans from the northeastern Alborz Range, Iran. *Rev. Palaeobot. Palynol.* 118, 77-99.
- Ghavidel-Syooki, G., Hassanzadeh, J., Vecoli, M., 2011. Palynology and isotope geochronology of the Upper Ordovician–Silurian successions (Ghelli and Soltan Maidan Formations) in the Khoshyeilagh area, eastern Alborz Range, northern Iran; stratigraphic and palaeogeographic implications. *Rev. Palaeobot. Palynol.* 164, 251-271.

- Hawkesworth, C.J., Mantovani, M.S.M., Peate, D.W., 1988. Lithosphere remobilization during Parana CFB magmatism. In: Cox, K.G., Menzies, M.A. (Eds.), *Oceanic and continental lithosphere: similarities and differences*. J. Petrol. Special volume, 205-223.
- He, Q., Xiao, L., Balta, B., Gao, R., Chen, J., 2010. Variety and complexity of the Late-Permian Emeishan basalts: Reappraisal of plume-lithosphere interaction process. *Lithos* 119, 91-107.
- Horton, B.K., Hassanzadeh, J., Stockli, D.F., Axen, G.J., Gillis, R.J., Guest, B., Amini, A., Fakhari, M.D., Zamanzadeh, S.M., Grove, M., 2008. Detrital zircon provenance of Neoproterozoic to Cenozoic deposits in Iran: Implications for chronostratigraphy and collisional tectonics. *Tectonophysics* 451, 97-122.
- Hosseini, S.H., Sadeghian, M., Zhai, M., Ghasemi, H., 2015. Petrology, geochemistry and zircon U-Pb dating of Band-e-Hezarchah metabasites (NE Iran): An evidence for back-arc magmatism along the northern active margin of Gondwana. *Chem. Erde*. 75, 207-218.
- Jenny, J., 1977. *Géologie et stratigraphie de Elburz oriental entre Aliabad et Shahrud, Iran*. Thèse Université de Genève, 238 p (Unpublished)
- Jung, S., Hoernes, S., 2000. The major- and trace-element and isotope (Sr, Nd, O) geochemistry of Cenozoic alkaline rift-type volcanic rocks from the Rhon area (central Germany): petrology, mantle source characteristics and implications for asthenosphere-lithosphere interactions. *J. Volc. Geotherm. Res.* 99, 27-53.
- Karimpour, M.H., Stern, C.R., Farmer, G.L., 2010. Zircon U-Pb geochronology, Sr-Nd isotope analyses, and petrogenetic study of the Dehnow diorite and Kuhsangi granodiorite (Paleo-Tethys), NE Iran. *J. Asian Earth Sci.* 37, 384-393.
- Lasemi, Y., 2001. Facies analysis, depositional environments and sequence stratigraphy of the Upper Pre-Cambrian and Paleozoic rocks of Iran. *Iran Geol. Surv. Publ.* 180 p (in Persian).
- Lustrino, M., Melluso, L., Morra, V., 2002. The transition from alkaline to tholeiitic magmas: a case study from the Orosei-Dorgali Pliocene volcanic district (NE Sardinia, Italy). *Lithos* 63, 83-113.
- Menzies, M.A., Rogers, N., Tindle, A., Hawkesworth, C.J., 1987. Metasomatic and enrichment processes in lithospheric peridotites, an effect of asthenosphere-lithosphere interaction. In: Menzies, M.A., Hawkesworth, C.J. (Eds.), *Mantle Metasomatism*. Academic Press, London, pp. 313-361.

- Muttoni, G., Mattei, M., Balini, M., Zanchi, A., Gaetani, M., Berra, F., 2009. The drift history of Iran from the Ordovician to the Triassic. In: BRUNET, M.-F., WILMSEN, M., GRANATH, J. W. (eds) South Caspian to Central Iran Basins. Geol. Soc. London. Spec. Publ. 312, 7-29.
- Pearce, J.A., Cann, J.R., 1973. Tectonic setting of basic volcanic rocks determined using trace element analysis. *Earth Planet. Sci. Lett.* 19, 290-300.
- Pearce, J.A., Norry, M.J., 1979. Petrogenetic implications of Ti, Zr, Y and Nb variations in volcanic rocks. *Contrib. Mineral. Petrol.* 69, 33-47.
- Rolland, Y., Billo, S., Corsini, M., Sosson, M., Galoyan, G., 2009. Blueschists of the Amassia-Stepanavan Suture Zone (Armenia): linking Tethys subduction history from E-Turkey to W-Iran. *Int. J. Earth Sci.* 98, 533-550.
- Saccani, E., Dilek, Y., Marroni, M., Pandolfi, L., 2015. Continental margin ophiolites of Neotethys: Remnants of Ancient Ocean-Continent Transition Zone (OCTZ) lithosphere and their geochemistry, mantle sources and melt evolution patterns. *Episodes* 38, 230-249.
- Saunders, A.D., Tarney, J., 1984. Geochemical characteristics of basaltic volcanism within back-arc basins. In: Kokelaar B. P. and Howells M. F. (eds), *Marginal basin geology*, Geol. Soc. London. Spec. Publ. 16, 59-76.
- Saunders, A.D., Norry, M.J., Tarney, J., 1988. Origin of MORB and chemically depleted mantle reservoirs: trace element constraints. *J. Petrol. Special Lithosphere Issue*, 415-445.
- Saunders, A.D., Storey, M., Kent, R.W., Norry, M.J., 1992. Consequences of plume lithosphere interactions. In: Storey, B.C., Alabaster, J., Pnakhurst, R.J. (Eds.), *Magmatism and the causes of continental break-up*. Geol. Soc. London. Spec. Publ. 68, 41-60.
- Sengör, A.M.C., 1987. Tectonics of the Tethysides: orogenic collage development in a collisional setting. *Annu. Rev. Earth Planet. Sci.* 15, 213-244.
- Shafaii Moghadam, H., Stern, R.J., 2014. Ophiolites of Iran: Keys to understanding the tectonic evolution of SW Asia: (I) Paleozoic ophiolites. *J. Asian Earth Sci.* 91, 19-38.
- Song, Y., Frey, F.A., Zhi, X., 1990. Isotopic characteristics of Hannuoba basalts, eastern China: implications for their petrogenesis and the composition of subcontinental mantle. *Chem. Geol.* 85, 35-52.
- Song, X.Y., Qi, H.W., Robinson, P.T., Zhou, M.F., Cao, Z.M., Chen, L.M., 2008. Melting of the subcontinental lithospheric mantle by the Emeishan mantle plume: evidence from the basal alkaline basalts in Dongchuan, Yunnan, Southwestern China. *Lithos* 100, 93-111.

- Stampfli, G.M., 1978. Etude géologique générale de l'Elbourz oriental au sud de Gonbad-e-Qabus (Iran NE). PhD thesis, Université de Genève, 329 p.
- Stampfli, G.M., Marcoux, J., Baud, A., 1991. Tethyan margins in space and time. In: Channell, J.E.T., Winterer, E.L., Jansa, L.F. (Eds.), *Paleogeography and Paleooceanography of Tethys*. *Palaeogeogr Palaeocl.* 87, 373-409.
- Stampfli, G.M., Raumer, J.F.V., Borel, G.D., 2002. Paleozoic evolution of pre-Variscan terranes: From Gondwana to the Variscan collision. In: MARTINEZ CATALAN, J.R., HATCHER, R.D., Jr., ARENAS, R. & DIAZ GARCIA, F. (Eds), *Variscan- Appalachian dynamics: The building of the late Paleozoic basement*. *Geol. Soc. Am. Bull.* 364, 263-280.
- Stocklin, J., 1968. Structural history and tectonics of Iran: a review. *Am Assoc Pet Geol Bull.* 52, 1229-1258.
- Sun, S.S., 1980. Lead isotopic study of young volcanic rocks from mid-ocean ridges, ocean islands and island arcs. *Phil. Trans. R. Soc. Lond.* A297, 409-445.
- Sun, S.S., McDonough, W.F., 1989. Chemical and isotopic systematics of oceanic basalts: implications for mantle composition and processes. In: Saunders, A.D., Norry, M.J. (Eds.), *Magmatism in the Ocean Basins*. *Geol Soc Spec Publ.* 42, 313-345.
- Tatsumoto, M., Nakamura, Y., 1991. DUPAL anomaly in the Sea of Japan: Lead, neodymium, and strontium isotopic variations at the eastern Eurasian continental margin. *Geochim. Cosmochim. Acta* 55, 3697-3708.
- Thompson, R.N., 1982. British Tertiary volcanic province. *Scott. J. Geol.* 18, 49-107.
- Turner, S., Arnaud, N., Liu, J., 1996. Post-collision, shoshonitic volcanism on the Tibetan Plateau: implications for convective thinning of the lithosphere and the source of ocean island basalts. *J. Petrol.* 37, 45-71.
- Weaver, B.L., 1991. Trace element evidence for the origin of ocean-island basalts. *Geology* 19, 123-126.
- Wilson, M., 1989. *Igneous petrogenesis: A global tectonic approach*. Unwin Hyman. London. 466 p.
- Winchester, J.A., Floyd, P.A., 1977. Geochemical discrimination of different magma series and their differentiation products using immobile elements. *Chem. Geol.* 20, 325-342.
- Yang, Y., Zhang, H., Chu, Z., Xie, L., Wua, F., 2010. Combined chemical separation of Lu, Hf, Rb, Sr, Sm and Nd from a single rock digest and precise and accurate isotope determinations

of Lu-Hf, Rb-Sr and Sm-Nd isotope systems using multi-collector ICP-MS and TIMS. *Int. J. Mass Spectrom.* 290, 120-126.

Zanchi, A., Zanchetta, S., Berra, F., Mattei, M., Garzanti, E., Molyneux, S., Nawab, A., Sabouri, J., 2009. The Eo-Cimmerian (Late? Triassic) orogeny in north Iran. In: Brunet, M.-F., Wilmsen, M. & Granath, J. W. (eds) *South Caspian to Central Iran Basins*. Geol. Soc. London. Spec. Publ. 312, 31-55.

Zindler, A., Hart, S., 1986. Chemical geodynamics. *Annu. Rev. Earth Planet. Sci.* 14, 493-571.

Figure Captions

Fig. 1. (a) Geological-structural map and major tectonic divisions of Iran (modified from Stocklin, 1968); (b) Sketch geographic map and location of studied sections; Simplified geological maps of main outcrops of the SMBC in the (c) Kaludar Valley (d) Cheshmeh-Seyed Valley and (e) around the village of Khoshyeilaq.

Fig. 2. Stratigraphic section of the SMBC, upper part of Ghelli Formation and lower part of Padeha Formation in the Cheshmeh-Seyed Valley, northwest of Qaleh-e-Nowkhareqan village. See text for further explanation.

Fig. 3. Some of the identified palynomorphs in the sedimentary interlayers (C1 and C2 shale units, see Fig. 2) of Cheshmeh-Seyed Valley section. Palynomorph assemblages in these shale units indicate a Late Ordovician age for middle and lower parts of the SMBC. (a) *Ancyrochitina merga* (b) *Leiosphaeridia* sp. (c) *Dactylofusa cabottii* (d) *Veryhachium reductum* (e) *Veryhachium trispinosum* (f & g) *Ordovicidium elegantulum* (h) *Veryhachium lairdii* group (i) *Diexallophosis*

denticulate (j) *Baltisphaeridium perclarum* (k) *Multiplicisphaeridium bifurcatum* (l) *Multiplicisphaeridium irregular*.

Fig. 4. Photomicrographs of thin sections of Soltan Maidan basaltic rocks under cross-polarized light. (a) Porphyritic texture and glomeroporphyritic cluster of clinopyroxene (Cpx) and plagioclase (Plg) crystals in the fine-grained plagioclase and opaque (Opq) groundmass. (b) A large clinopyroxene (augite) phenocryst in a groundmass of plagioclase and clinopyroxene (augite). (c) Subhedral phenocrysts of olivine (Ol) are entirely replaced by calcite (Cc) and opaque minerals. (d) Amygdaloidal texture. Filling minerals are calcite and chlorite.

Fig. 5. Classification of Soltan Maidan volcanic rocks in terms of Zr/TiO_2 versus Nb/Y (after Winchester and Floyd, 1977). As shown, samples mostly plot near the boundary line dividing alkaline and subalkaline basalts.

Fig. 6. Plot of La/Lu versus La (after Lustrino et al., 2002) to illustrate variations in degrees of partial melting in the source.

Fig. 7. Plots of (a) Zr versus Nb and (b) Y, and (c) Nb/La versus SiO_2 for the Soltan Maidan basaltic samples. Two different trends of FC and AFC are marked. The trends for FC and AFC are from Dong et al. (2010). See text for details.

Fig. 8. Plots of (a) $1/\text{Sr}$ versus $^{87}\text{Sr}/^{86}\text{Sr}$ and (b) $1/\text{Nd}$ versus $^{143}\text{Nd}/^{144}\text{Nd}$ and (c-d) SiO_2 contents versus initial $^{87}\text{Sr}/^{86}\text{Sr}$ and $^{143}\text{Nd}/^{144}\text{Nd}$ ratios for the Soltan Maidan basalts. As shown, geochemical trends do not support AFC processes.

Fig. 9. (a) Chondrite- and (b) primitive-mantle normalized multi-element patterns of Soltan Maidan basaltic samples, OIB, E-MORB and N-MORB for comparison. Note that the samples patterns are more similar to the patterns of OIB. Chondrite values are from Thompson (1982), and primitive-mantle values from Sun and McDonough (1989). OIB data are after Sun (1980); Sun and McDonough (1989), E-MORB from Sun and McDonough (1989), and N-MORB values are from Sun (1980); and Saunders and Tarney (1984).

Fig. 10. Discrimination diagrams for Soltan Maidan basaltic samples. (a) Zr/Y versus Zr diagram is after Pearce and Norry (1979) and (b) $\text{Ti}-\text{Zr}-\text{Y}$ diagram is from Pearce and Cann (1973). (c) OIB and MORB values are from Sun and McDonough (1989). Abbreviations: MORB= mid-ocean ridge basalt, IAT= island arc tholeiite, CAB= calc-alkali basalt.

Fig. 11. $^{143}\text{Nd}/^{144}\text{Nd}$ versus $^{87}\text{Sr}/^{86}\text{Sr}$ diagram for the Soltan Maidan basalts in eastern Alborz. The fields of DM, MORB, HIMU, PREMA, BSE, OIB, EM1 and EM2 are from Zindler and Hart (1986).

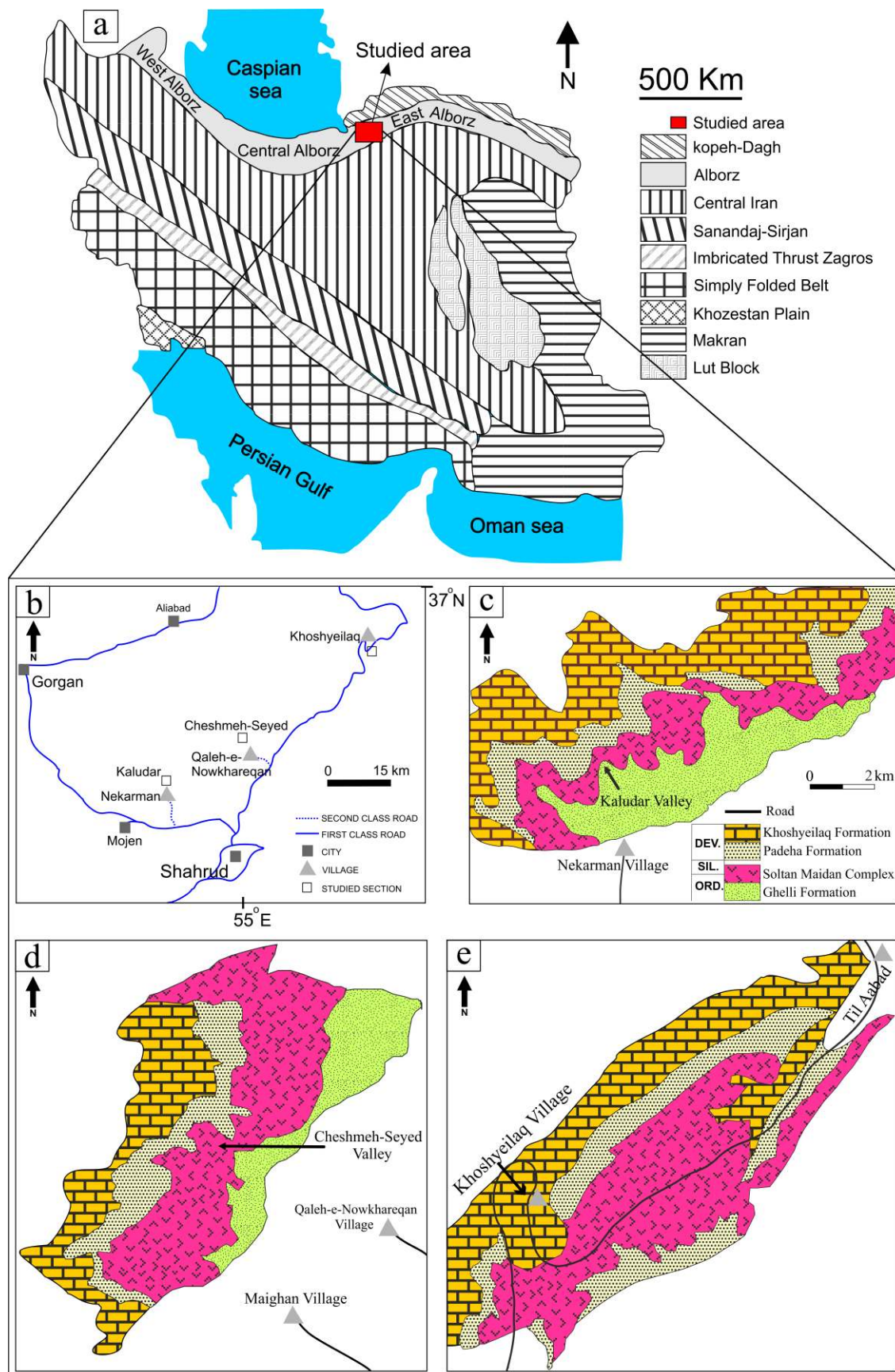
Fig. 12. Schematic tectono-magmatic model of the study area during the Late Ordovician to Middle Devonian time. See text for further explanation.

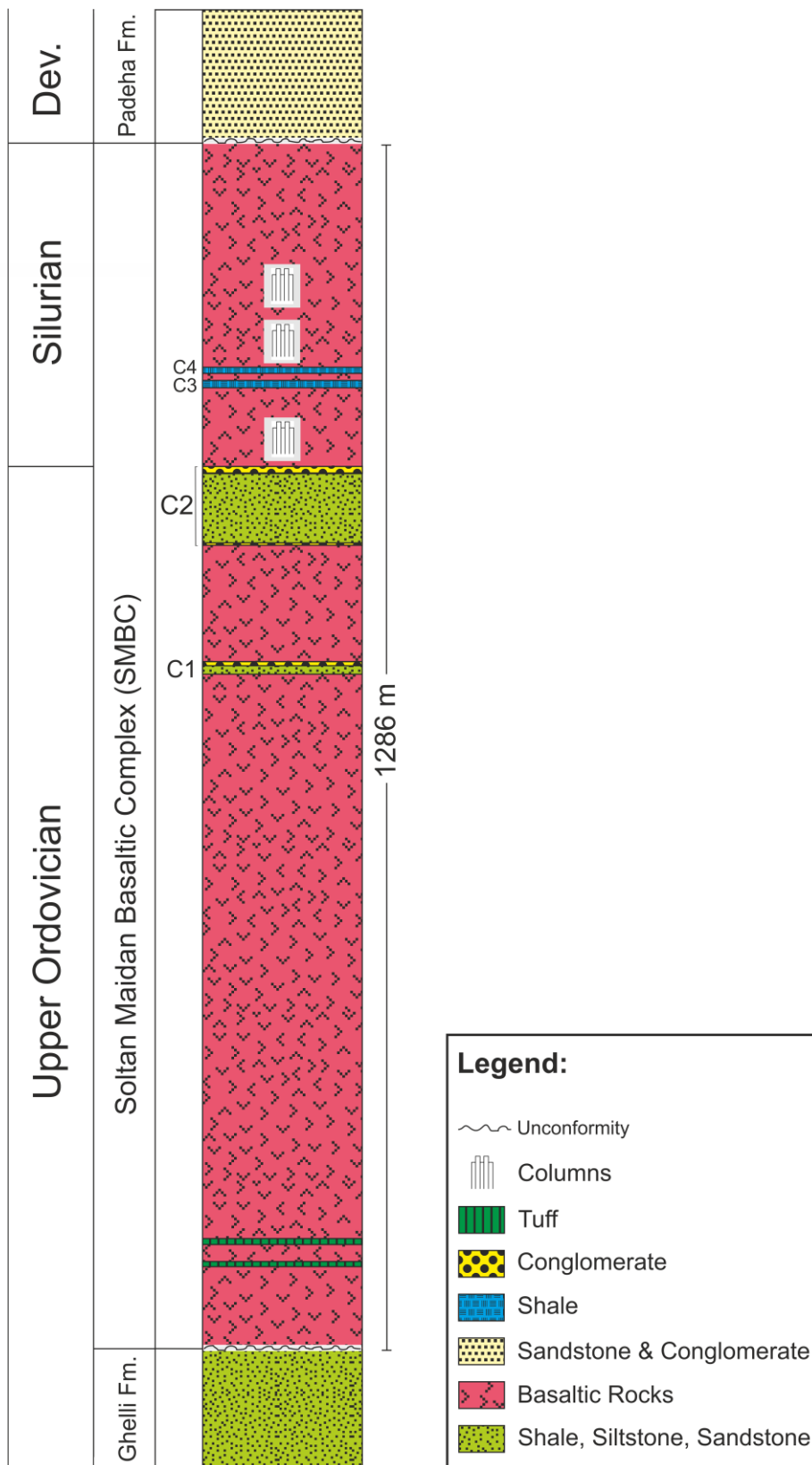
Tables

Table 1. Whole-rock analytical results of major (%) and trace elements (ppm) for Soltan Maidan basalts.

Table 2. Sr-Nd isotope data of the basalts from SMBC, eastern Alborz.

Table 3. Representative incompatible trace element ratios of Soltan Maidan basalts, and primitive mantle, N-MORB, E-MORB, continental crust, HIMU-OIB, EM1-OIB and EM2-OIB for comparison. Data are after Saunders et al. (1988) and Weaver (1991).





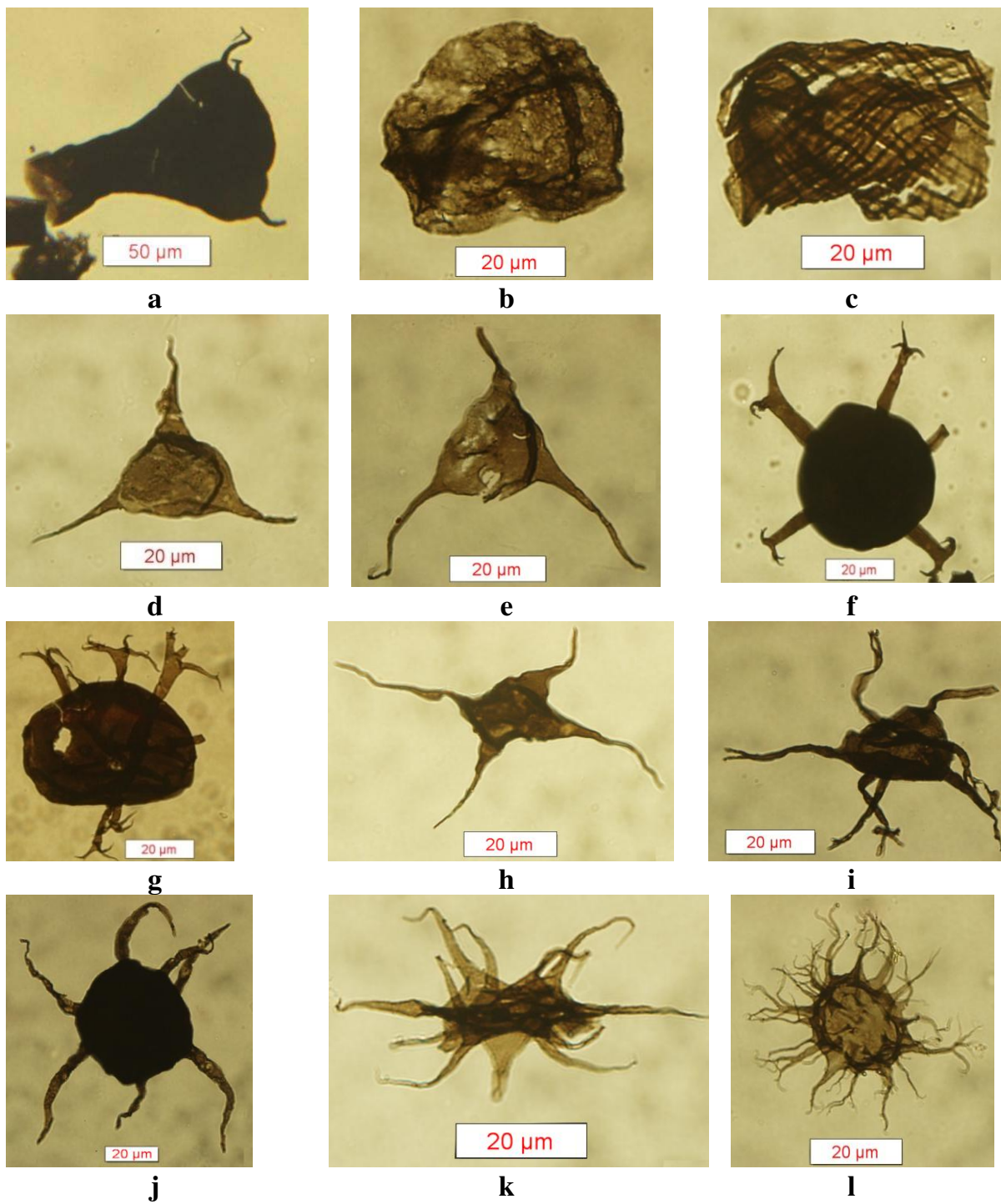


Fig. 3

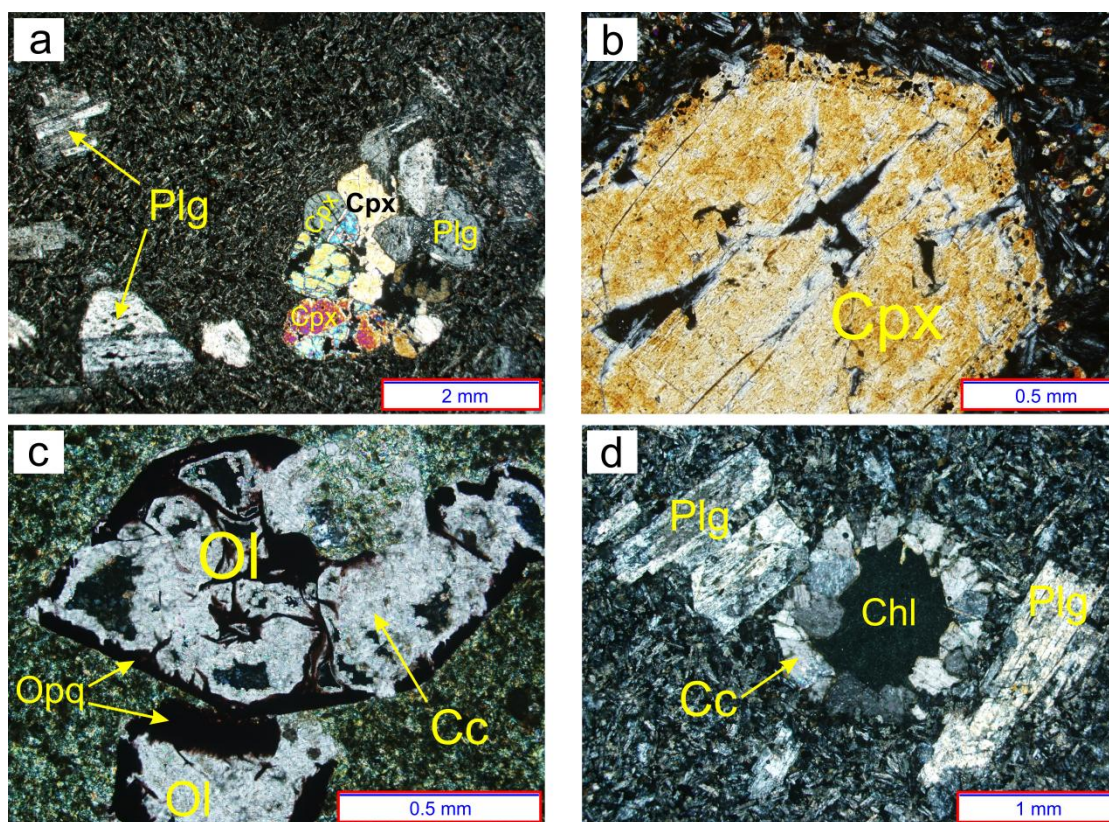
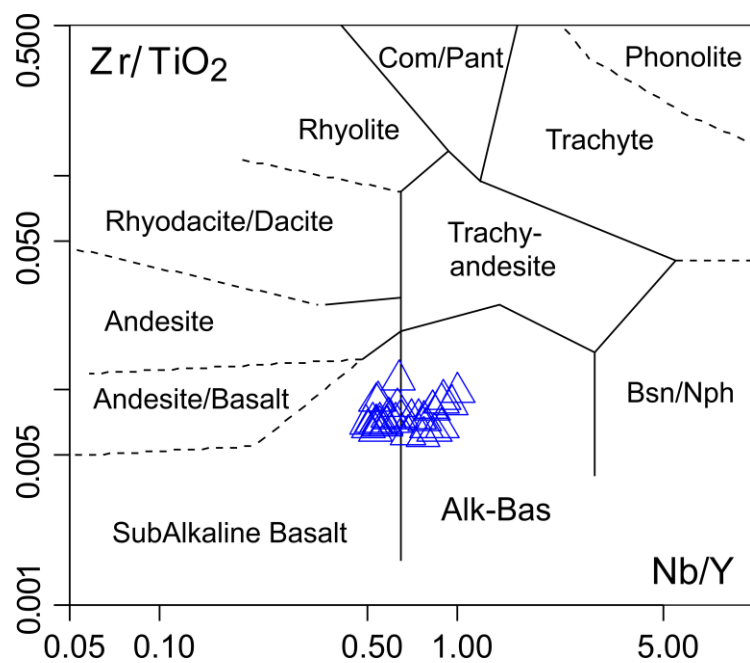
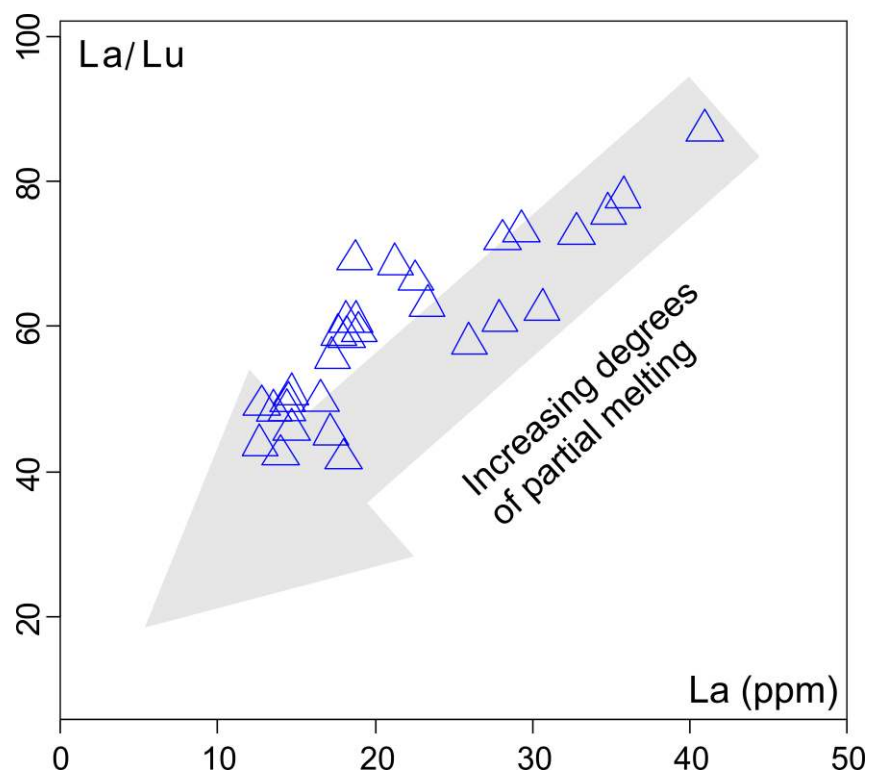
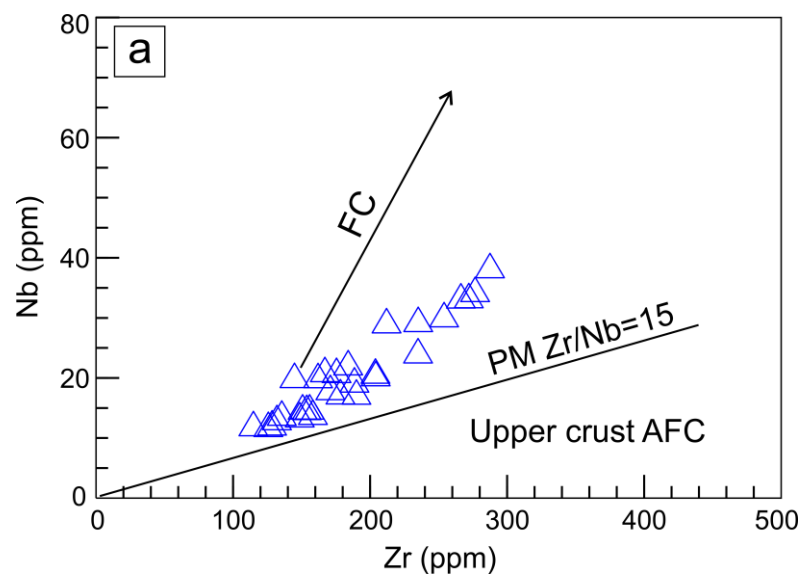
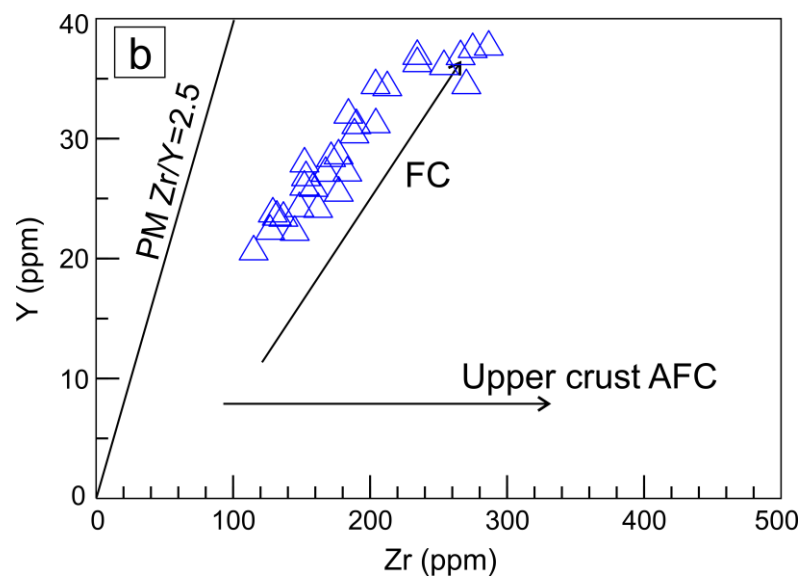


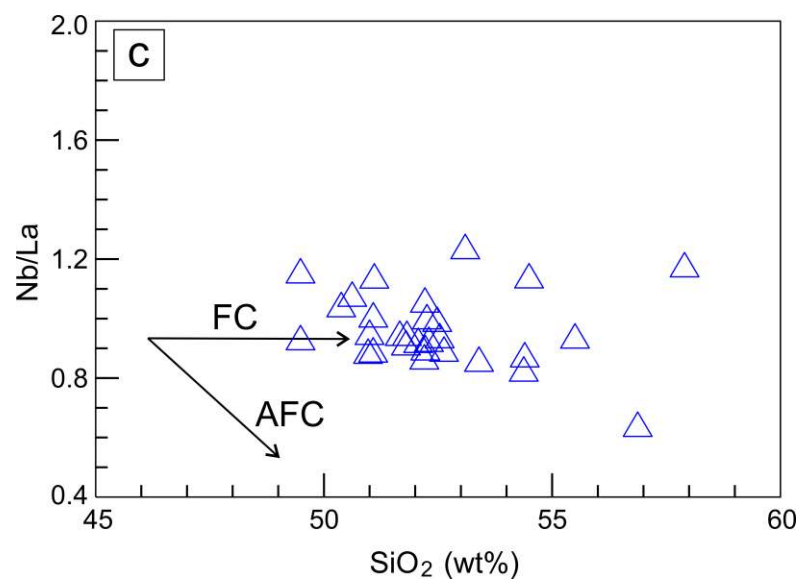
Fig. 4

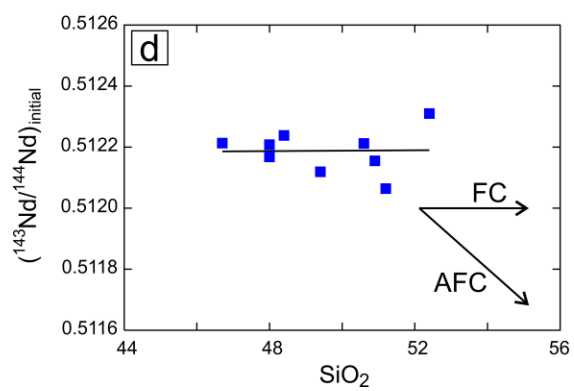
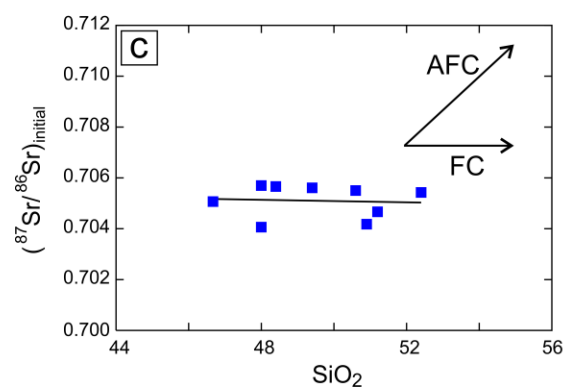
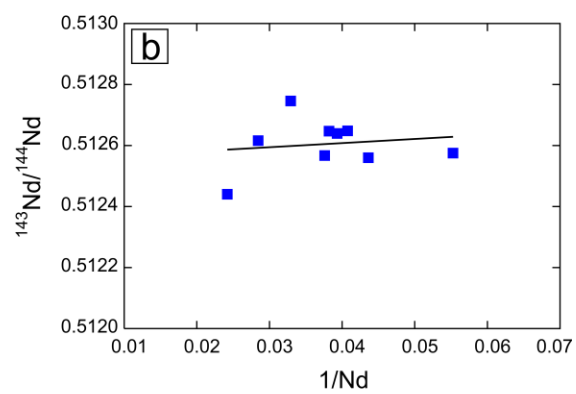
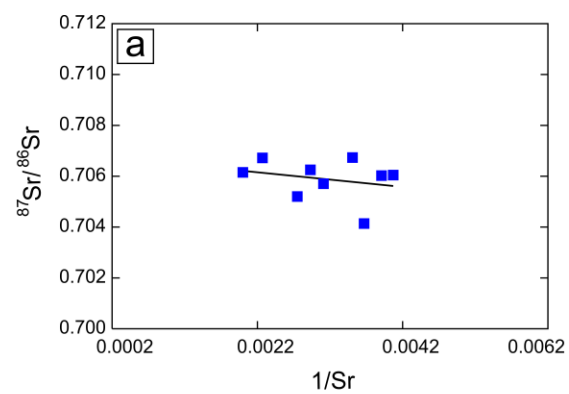


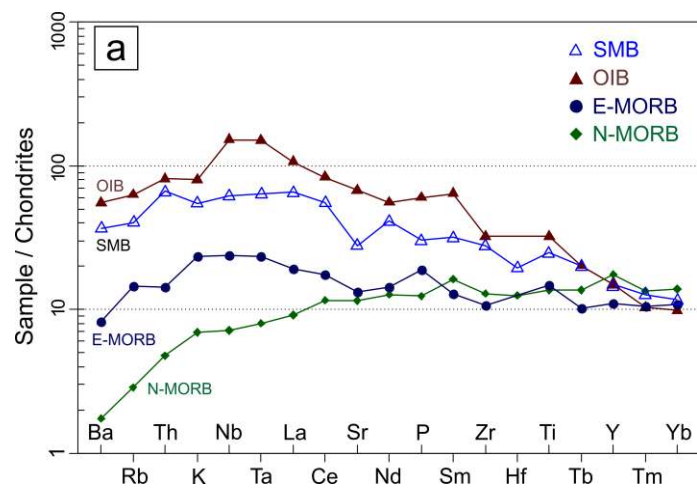


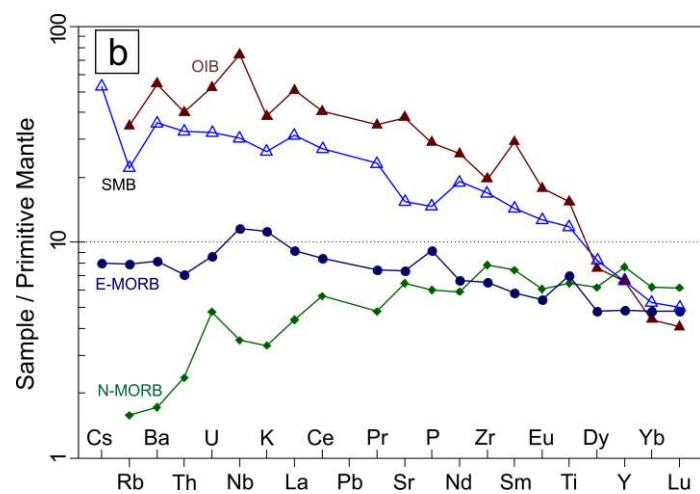


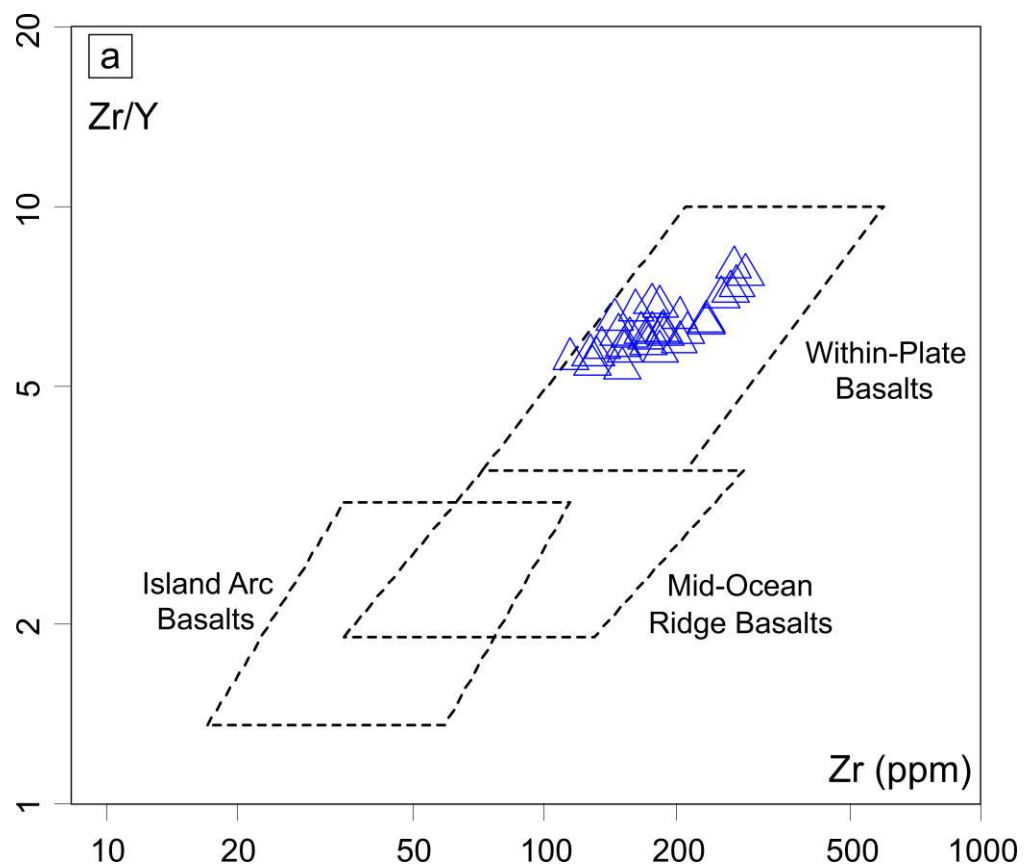


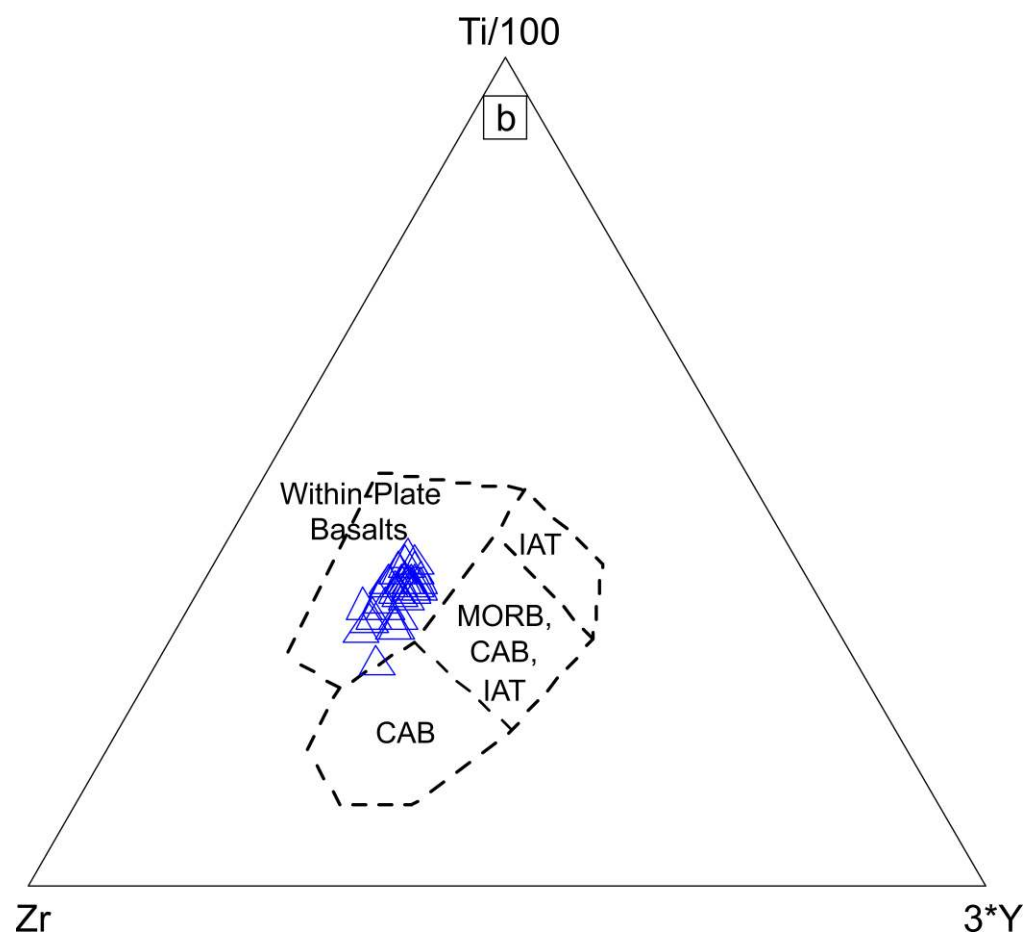


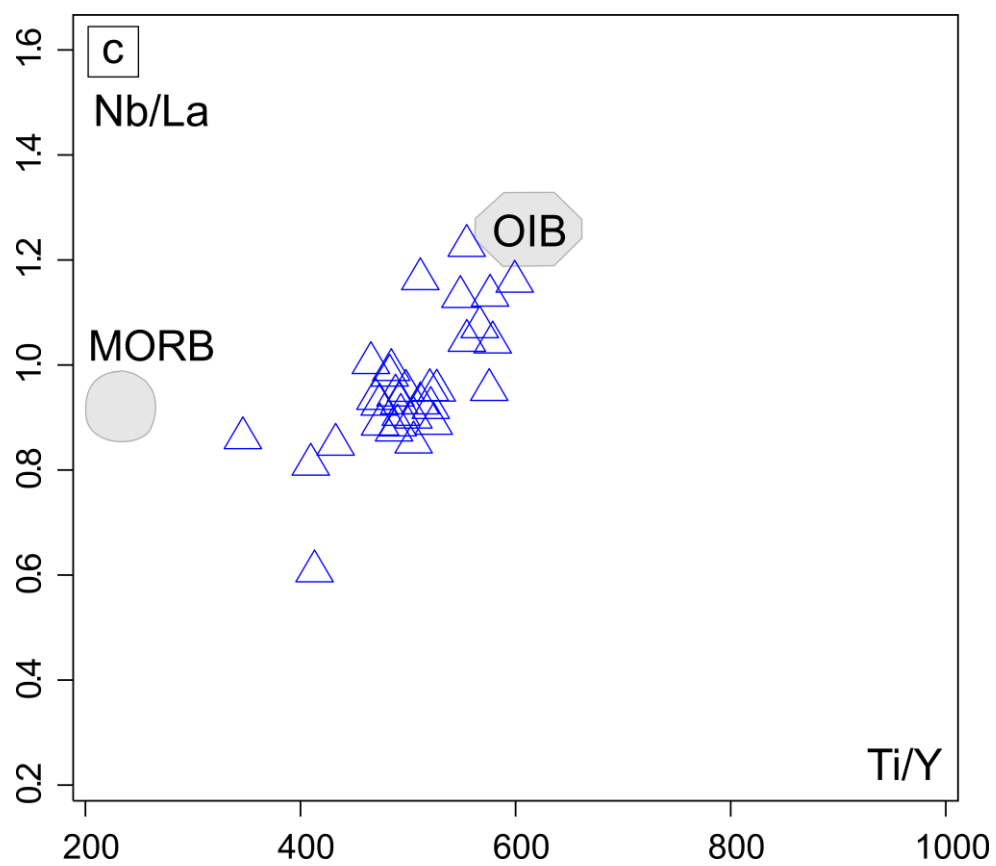


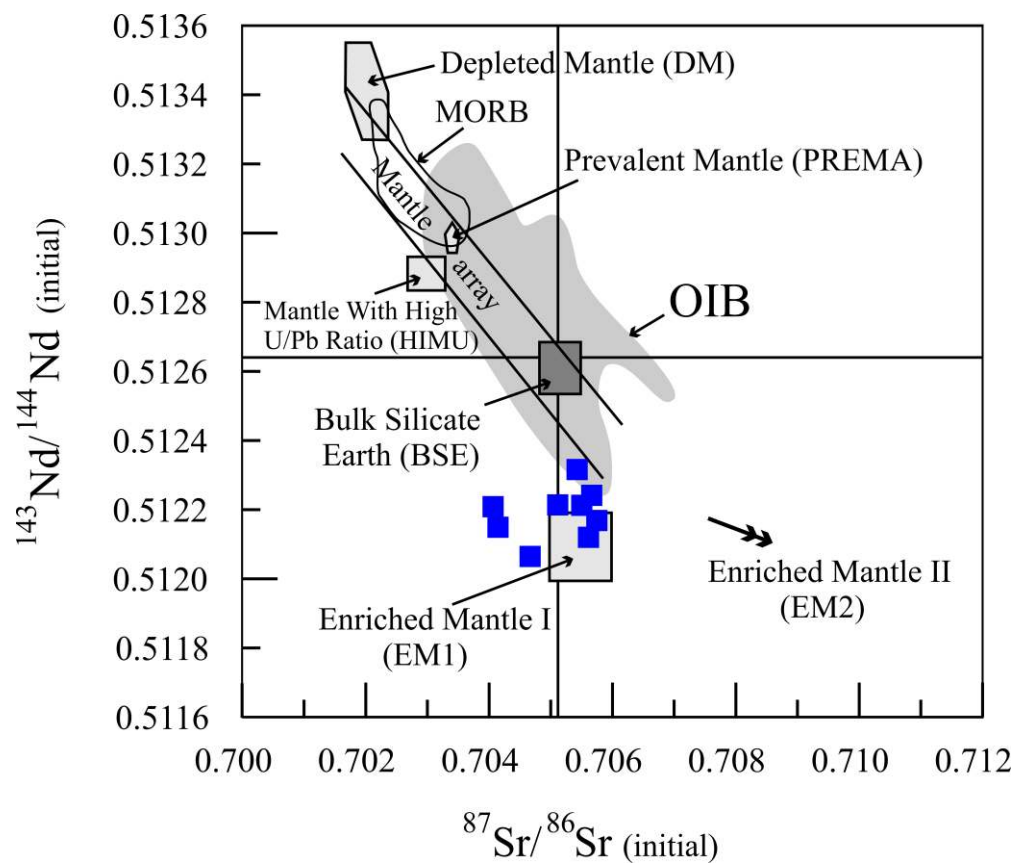


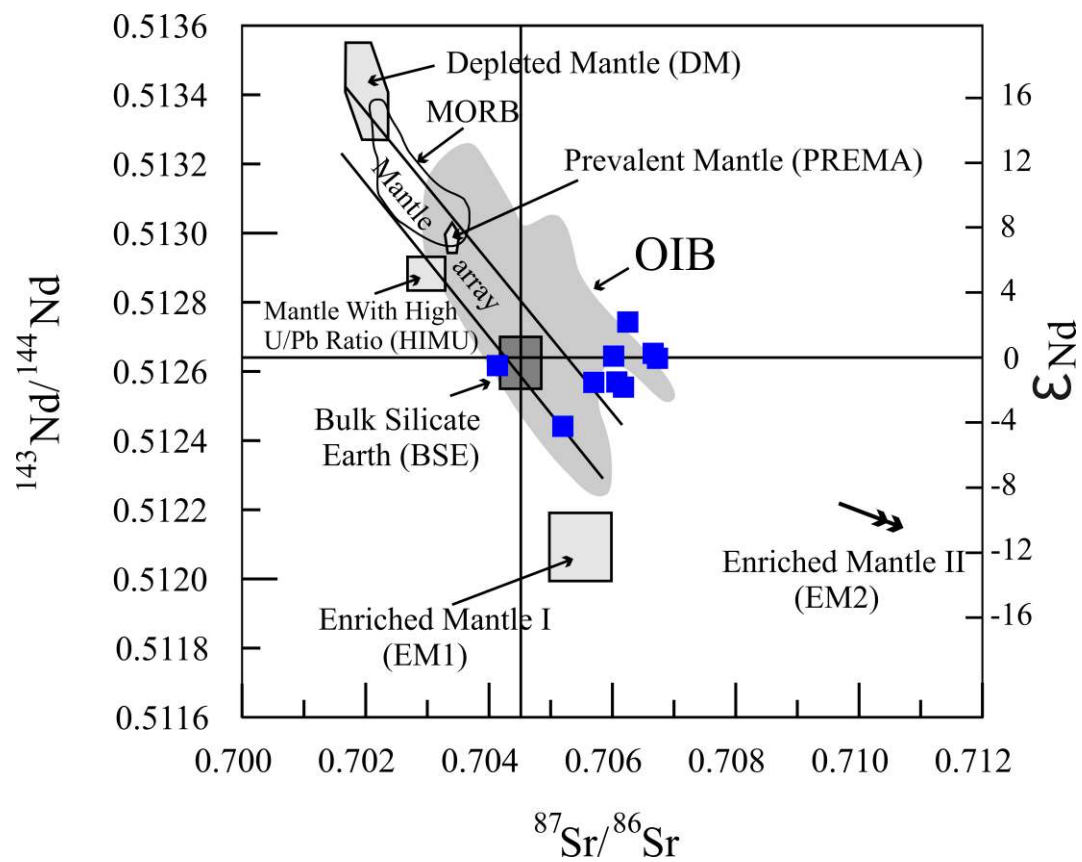


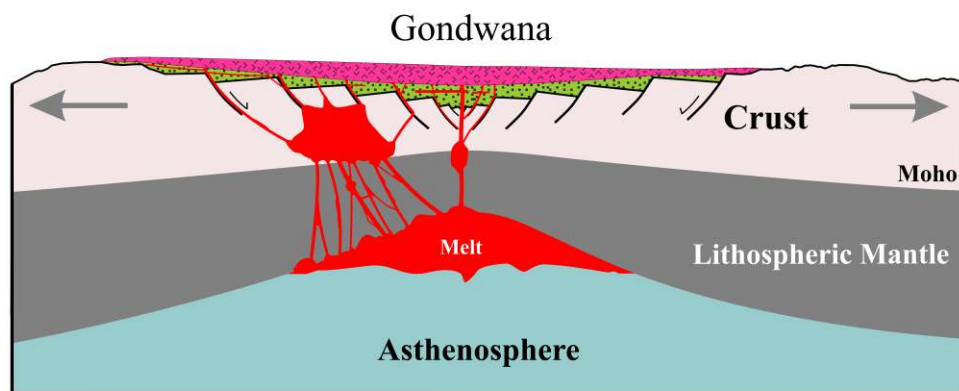




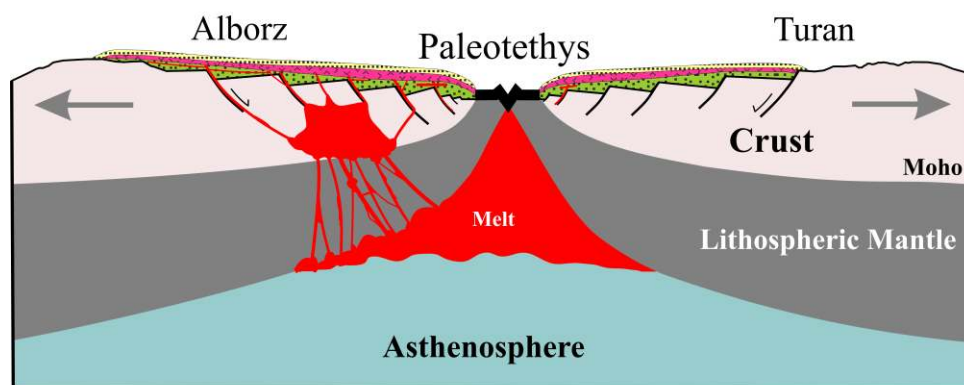








Late Ordovician-Late Silurian



Late Silurian-Middle Devonian

Soltan Maidan Basaltic Complex
 Ghelli Formation
 Padeha Formation

Table 1

Location	Kaludar Valley										Cheshmeh-Seyed Valley				
Sample	K 1A	K 2B	K 3D	K 5A	K 7B	K 10A	K 11B	K 13A	K 17A	K 19A	M 2D	M 2G	M 5B	M 7B	M 10C
SiO ₂	51.2	50.4	52.2	48.0	51.4	47.5	51.5	50.8	48.5	55.2	48.1	49.5	48.4	48.8	49.2
TiO ₂	2.95	2.89	3	2.02	2.46	1.61	1.68	2.1	2.07	2.8	1.86	2.8	2.31	2.03	1.87
Al ₂ O ₃	13.3	13.3	13.2	15.6	14	12.7	14.5	13.6	13.5	14.2	14.2	13	14.3	13.5	13.5
Fe ₂ O _{3 (t)}	13.7	12.5	11.8	10.2	11.9	12.6	9.68	11.9	12.5	8.38	11.5	13.6	11.7	11.7	11.4
MnO	0.23	0.17	0.34	0.27	0.26	0.24	0.19	0.23	0.22	0.16	0.22	0.2	0.25	0.18	0.18
MgO	4.2	4.24	4.84	5.57	5.2	10.1	6.07	6.37	6.1	4.23	6.32	4.5	5.84	6.63	6.4
CaO	7.88	8.69	4.74	7.47	9.43	8.27	6.25	8.09	8.03	4.01	7.3	6.76	7.9	9.18	8.11
Na ₂ O	2.7	2.5	5.1	4.1	2.5	1.8	3.5	3	2.6	5.9	3.6	3.9	3.5	2.7	3.2
K ₂ O	0.86	0.81	0.2	0.55	0.95	0.99	1.11	0.83	1.26	0.18	0.79	0.66	1.1	0.77	1.05
P ₂ O ₅	0.48	0.45	0.44	0.23	0.3	0.16	0.19	0.21	0.19	0.29	0.2	0.38	0.27	0.21	0.17
LOI	1.88	2.11	2.59	3.35	1.4	3.39	3.72	2.66	2.61	2.92	3.29	2.73	2.88	1.99	3.01
Total	99.38	98.06	98.45	97.36	99.8	99.36	98.39	99.79	97.58	98.27	97.38	98.03	98.45	97.69	98.09
Ba	350	310	80	110	250	280	370	240	640	60	190	160	310	210	500
Sr	370	360	280	500	350	270	440	410	340	300	320	210	440	310	360
Cs	0.6	0.3	0.2	0.4	0.2	1.3	0.9	0.2	0.7	0.1	0.4	0.2	1	0.2	0.2
Rb	10.5	10.3	3.7	12.2	13.8	14.9	22.1	18.2	22.7	3	22.9	14.7	26.7	13.5	26.2
Hf	6	6	7	3	4	2	3	3	3	5	3	7	4	3	2
Th	5	5	4.9	2.3	2.1	1.2	3.3	1.6	1.7	2.3	3	4.8	1.7	1.2	1.1
U	1.13	1.13	1.05	0.42	0.51	0.31	0.85	0.51	0.3	0.62	0.79	1.26	0.49	0.32	0.24
Zr	267	276	271	145	184	115	157	153	151	204	162	288	176	148	127
Nb	33	34	33	20	19	12	14	14	14	20	20	38	20	13	12
Ta	2	2.1	2.1	1.2	1.1	0.7	0.9	0.8	0.9	1.2	1.1	2.3	1.1	0.7	0.7
Ga	22	22	19	20	21	19	19	21	21	23	19	24	20	19	20
Y	37.1	37.5	34.3	22.4	27.1	20.7	26	26.8	28.1	34.5	24.2	37.5	25.6	24.3	22.5
Ni	24	124	33	41	37	218	55	68	38	70	75	42	68	90	75
V	315	318	324	265	264	221	212	253	258	312	253	295	284	246	251
Co	36.7	30.3	38.1	37	38	55.3	33.8	41.8	43.9	68	42.6	38	41.6	44.1	40.2
Zn	170	140	145	206	194	252	176	259	214	221	635	775	400	178	231
Cu	35	53	30	56	83	10	62	18	22	65	102	84	44	28	78
La	35.8	34.8	29.3	17.7	18.2	12.8	17.3	14.2	14	17.2	22.6	40.9	18.7	14.7	12.7
Ce	76.5	76.7	67.9	41.5	42.7	28.4	40.8	32.4	32.2	43.8	45.8	86.8	42.7	33.9	29.4
Pr	9.79	9.82	8.64	5.39	5.93	3.84	5.28	4.46	4.49	5.97	5.73	10.8	5.61	4.87	4.05
Nd	37.4	37.1	34.2	20.8	24.3	16	22.2	18.5	18.8	23.5	22.2	40.3	23	20	17.1
Sm	8.7	8.5	7.9	4.9	6.3	4	5.5	4.9	5.7	7	5.6	9.2	5.6	5.1	4.4
Eu	2.53	2.64	2.08	1.76	2.2	1.47	1.79	1.8	1.74	2.5	1.66	3.02	1.85	1.8	1.7
Gd	8.8	8.6	8.03	5.78	6.8	4.45	5.81	5.77	6.07	7.19	5.49	9.32	6.14	5.43	5.21
Tb	1.31	1.38	1.17	0.8	1	0.72	0.89	0.94	0.96	1.18	0.85	1.3	0.94	0.86	0.8
Dy	7.65	7.61	6.89	4.55	5.59	4.53	5.46	5.62	5.62	6.87	4.92	7.56	5.19	5.18	4.55
Ho	1.48	1.49	1.35	0.85	1.07	0.85	1.07	1.03	1.1	1.38	0.92	1.54	0.98	1.07	0.9
Er	4.09	4.08	3.88	2.56	3	2.19	2.77	2.8	2.85	3.29	2.46	4.15	2.8	2.65	2.45
Tm	0.55	0.54	0.46	0.32	0.4	0.25	0.38	0.34	0.41	0.48	0.35	0.56	0.39	0.34	0.33
Yb	3.5	3.4	2.9	2	2.3	1.7	2.3	2.1	2.4	2.6	2.1	3.4	2.2	1.9	2.1
Lu	0.46	0.46	0.4	0.3	0.31	0.26	0.31	0.3	0.33	0.38	0.34	0.47	0.27	0.32	0.29

Table 1 (continued)

Location		Khoshyeilaq area													
Sample	M 12A	M 16A	M 18A	M 21B	M 27	M 30	M 35	M42A	M44A	KH1A	KH2	KH3B	KH5C	KH9B	KHG4
SiO ₂	49.5	50.2	50.9	49.9	49.4	55.0	51.6	48.0	52.4	49.9	48.5	50.3	49.4	50.6	46.7
TiO ₂	1.89	1.77	1.95	2.1	1.83	2.07	2.93	3.16	1.74	2.99	3.34	2.81	2.24	2.53	2.56
Al ₂ O ₃	13.5	14.1	14.8	13.2	13.4	13.4	13.6	12.6	14.4	12.4	12.8	16.3	13.3	12.8	13.3
Fe ₂ O _{3 (t)}	11.3	11.1	10.9	12.6	11.3	11	10.2	14.7	11	14.2	14.9	11.1	12	13.5	13.6
MnO	0.17	0.18	0.19	0.21	0.19	0.16	0.21	0.22	0.19	0.26	0.19	0.11	0.2	0.3	0.25
MgO	6.31	5.55	4.88	5.72	5.87	3.64	5.35	4.78	4.37	3.98	3.96	2.8	5.75	5.34	6.02
CaO	8.2	8.98	7.14	8.22	7.76	6.69	4.2	9.03	6.67	7.78	7.07	4.41	7.46	6.16	7.52
Na ₂ O	3.3	2.4	2.8	2.6	4.3	2.9	4.4	2.3	4.4	2.9	2.7	6.5	3.3	3.4	3.7
K ₂ O	1.17	0.93	1.5	0.82	0.34	1.64	0.07	0.13	0.95	0.43	1.24	0.04	0.92	1	0.36
P ₂ O ₅	0.2	0.17	0.22	0.21	0.16	0.23	0.35	0.41	0.25	0.48	0.48	0.36	0.25	0.26	0.25
LOI	2.53	1.74	2.38	2.23	2.84	1.7	4.65	2.46	2.16	2.56	2.44	3.53	2.34	2.36	3.38
Total	98.07	97.12	97.66	97.81	97.39	98.43	97.56	97.79	98.53	97.88	97.62	98.26	97.16	98.25	97.64
Ba	310	220	340	220	90	390	60	110	450	270	300	40	250	290	160
Sr	350	350	320	290	240	300	220	270	340	350	280	150	320	280	440
Cs	0.5	0.3	0.4	0.2	0.2	0.4	0.2	0.8	0.2	0.3	0.1	0.1	0.2	0.2	0.1
Rb	20.6	18	26.6	13	5.8	38.1	1.5	1.1	15	7.1	16.6	0.7	19.8	19.7	5.5
Hf	3	2	4	3	3	4	5	5	5	5	5	4	4	4	4
Th	1.4	1.5	3	1.4	1.5	4.9	3.3	2.6	2.4	4	3.9	2.1	2	2.1	1.8
U	0.46	0.35	0.81	0.35	0.38	1.29	0.9	0.62	0.63	1.04	0.87	0.34	0.58	0.59	0.45
Zr	136	132	171	152	129	190	235	212	204	254	235	184	177	188	167
Nb	13	13	18	14	12	17	24	29	20	30	29	22	17	19	21
Ta	0.7	0.7	1	0.8	0.6	1.1	1.3	1.8	1.2	2.1	1.9	1.4	1.1	1.1	1.2
Ga	19	21	22	20	20	21	26	23	22	24	24	24	21	23	21
Y	23.5	23.5	28.4	26.1	23.8	31.1	37	34.4	31.3	36.1	36.6	32.1	28.7	30.4	27.2
Ni	70	62	36	53	41	27	26	27	40	14	6	24	67	39	31
V	246	235	241	267	233	259	341	325	174	268	311	277	274	307	329
Co	39.7	40.9	37.9	42.5	38.5	32	46.2	37.5	28.8	34.6	39	35.3	40.7	43.2	50.7
Zn	108	215	147	218	158	182	224	106	211	215	152	121	136	170	168
Cu	42	30	69	44	85	82	209	37	56	41	16	8	29	222	61
La	14.4	14.7	21.3	16.5	13.6	28.1	26	27.9	23.3	32.8	30.6	18	18.8	20.1	18.2
Ce	32.9	33.2	47	37.1	30	57.4	58.7	62.2	51.3	71	66.5	40.4	43.4	44	43.2
Pr	4.69	4.67	6.28	5.12	4.25	7.44	7.72	8.17	6.9	9.18	8.68	5.25	5.81	6.21	5.98
Nd	18.8	18.6	24.3	21.1	17.5	27.7	32.3	33.3	26.8	35.9	34.2	21.7	24.2	25	24.5
Sm	5	4.7	6.5	5.5	4.7	6.9	7.7	8.2	7.3	8.3	8.5	5.7	6	6.5	6
Eu	1.68	1.76	2.07	1.89	1.7	2.04	2.7	2.78	2.32	3.12	2.75	1.88	2.11	2.19	2.02
Gd	4.91	5.06	6.21	5.71	5.1	6.84	8.71	8.63	7.96	8.92	8.06	6.03	6.53	6.79	6.11
Tb	0.81	0.78	0.96	0.92	0.76	1.06	1.34	1.29	1.14	1.38	1.32	1	1.04	1.11	1.04
Dy	4.92	4.93	5.71	5.28	5.06	6.3	7.37	7.21	6.93	7.36	7.6	6.17	6.13	6.46	5.79
Ho	0.93	0.91	1.17	1.07	0.91	1.21	1.47	1.43	1.34	1.46	1.48	1.33	1.13	1.23	1.14
Er	2.73	2.31	2.96	2.48	2.4	3.47	3.9	3.84	3.38	3.79	3.71	3.71	3.14	3.3	2.7
Tm	0.33	0.37	0.45	0.36	0.34	0.5	0.5	0.47	0.52	0.48	0.54	0.43	0.41	0.45	0.38
Yb	2	2.1	2.5	2.2	2.1	2.7	3.1	3.1	2.9	3	3.2	2.9	2.5	2.7	2.2
Lu	0.29	0.29	0.31	0.33	0.28	0.39	0.45	0.46	0.37	0.45	0.49	0.43	0.31	0.34	0.3

Table 2

Sm-Nd Compositions								
Sample No.	Sm (ppm)	Nd (ppm)	$^{143}\text{Nd}/^{144}\text{Nd}$	$^{147}\text{Sm}/^{144}\text{Nd}$	$(^{143}\text{Nd}/^{144}\text{Nd})_i$	Error (2 σ)	ϵ_{Nd}	$\epsilon_{\text{Nd}}(t)$
K1	8.413	38.17	0.512440	0.1334	0.512064	0.000013	-3.86	-0.38
K2	5.035	21.92	0.512560	0.1390	0.512168	0.000013	-1.52	1.65
Kh1	6.123	24.29	0.512643	0.1526	0.512213	0.000012	0.10	2.52
Kh2	6.343	24.87	0.512647	0.1544	0.512212	0.000012	0.17	2.50
M1	5.689	23.48	0.512651	0.1467	0.512238	0.000011	0.25	3.00
M2	6.110	25.25	0.512567	0.1465	0.512155	0.000011	-1.38	1.38
M3	4.666	17.46	0.512575	0.1618	0.512119	0.000013	-1.23	0.69
M4	7.870	32.84	0.512616	0.1451	0.512208	0.000010	-0.42	2.42
M5	7.240	28.64	0.512746	0.1531	0.512315	0.000011	2.10	4.50
Rb-Sr Compositions								
Sample No.	Rb (ppm)	Sr (ppm)	$^{87}\text{Sr}/^{86}\text{Sr}$	$^{87}\text{Rb}/^{86}\text{Sr}$	$(^{87}\text{Sr}/^{86}\text{Sr})_i$	Error (2 σ)	ϵ_{Sr}	$\epsilon_{\text{Sr}}(t)$
K1	11.02	363.7	0.705200	0.0877	0.704663	0.000011	9.94	9.51
K2	12.80	501.0	0.706150	0.0739	0.705697	0.000011	23.41	24.19
Kh1	13.19	256.0	0.706023	0.1491	0.705110	0.000010	21.63	15.86
Kh2	19.81	285.0	0.706733	0.2011	0.705501	0.000011	31.69	21.41
M1	26.33	441.1	0.706718	0.1728	0.705660	0.000009	31.49	23.67
M2	27.63	321.4	0.705702	0.2488	0.704178	0.000014	17.06	2.63
M3	6.023	245.8	0.706043	0.0709	0.705609	0.000011	21.91	22.95
M4	1.161	272.3	0.704138	0.0123	0.704062	0.000010	-5.14	0.98
M5	15.92	341.7	0.706250	0.1348	0.705424	0.000014	24.84	20.33

Initial Sr and Nd isotope ratios along with the epsilon values were calculated assuming an eruption age of 430 Ma.

Chondrite Uniform Reservoir (CHUR) values $^{87}\text{Rb}/^{86}\text{Sr}=0.0827$, $^{87}\text{Sr}/^{86}\text{Sr}=0.7045$, $^{147}\text{Sm}/^{144}\text{Nd}=0.1967$, and $^{143}\text{Nd}/^{144}\text{Nd}=0.512638$ were used for the initial Sr and Nd isotope calculation.

Table 3

	Zr/Nb	La/Nb	Ba/Nb	Ba/Th	Th/Nb	Th/La	Ba/La	Rb/Nb
Primitive mantle	14.8	0.94	9	77	0.117	0.125	9.6	0.91
N-MORB	30	1.07	1.7-8	60	0.025-0.071	0.067	4	0.36
E-MORB	-	-	4.9-8.5	-	0.06-0.08	-	-	-
Continental crust	16.2	2.2	54	124	0.44	0.204	25	4.7
HIMU-OIB	3.2-5	0.66-0.77	4.9-6.9	49-77	0.078-0.101	0.107-0.133	6.8-8.7	0.35-0.38
EM1-OIB	4.2-11.5	0.86-1.19	11.4-17.8	103-154	0.105-0.122	0.107-0.128	13.2-16.9	0.88-1.17
EM2-OIB	4.5-7.3	0.89-1.09	7.3-13.3	67-84	0.111-0.157	0.122-0.163	8.3-11.3	0.59-0.85
Soltan Maidan Basalts	7.3-11.4	0.82-1.65	1.8-45.7	16-455	0.085-0.288	0.082-0.191	2.3-45.7	0.03-2.24
(Average)	(9.46)	(1.06)	(14.6)	(122)	(0.128)	(0.119)	(13.4)	(0.88)